Retinal Configuration of *pp*R Intermediates Revealed by Photo-Irradiation Solid-State NMR and DFT

Yoshiteru Makino,[1] Izuru Kawamura,[1,*] Takashi Okitsu,[2] Akimori Wada,[2] Naoki Kamo,[3] Yuki Sudo,[4] Kazuyoshi Ueda,[1,*] and Akira Naito[1,*]

[1]Graduate School of Engineering, Yokohama National University, Hodogaya-ku, Yokohama 240-8501, Japan; [2]Laboratory of Organic Chemistry for Life Science, Kobe Pharmaceutical University, Higashinada-ku, Kobe 658-8558, Japan; [3]Faculty of Advanced Life Science, Hokkaido University, Kita-ku, Sapporo 060-0810, Japan; [4]Graduate School of Medicine, Dentistry and Pharmaceutical Sciences, Okayama University, Okayama 700-8530, Japan.

Running title: retinal structure of *pp*R intermediates

***Corresponding Authors**

A.N. : naito@ynu.ac.jp,

I.K. : izuruk@ynu.ac.jp,

K.U.: ueda-kazuyoshi-cz@ynu.ac.jp

KEYWORDS:

Retinal, *Pharaonis* phoborhodpsin, *in-situ* photo-irradiation solid-state NMR

ABSTRACT

Pharanois phoborhodopsin (*p*pR) from *Natronomonas pharaonis* is a transmembrane photoreceptor protein involved in negative phototaxis. Structural changes in *p*pR triggered by photoisomerization of the retinal chromophore are transmitted to its cognate transducer protein (*p*HtrII) through a cyclic photo-reaction pathway involving several photointermediate. This pathway is called the photo-cycle. It is important to understand the detailed configurational changes of retinal during the photo-cycle. We previously observed one of the photointermediates (M-intermediates) by *in-situ* photo-irradiation solid-state NMR experiments (Y. Tomonaga et al., Biophys. J., **2011**, 101, L50-L52). In this study, we further observed the ^{13}C CP MAS NMR signals of late photointermediates such as O- and N'-intermediates by illuminating with green light (520 nm). Under blue light (365 nm) irradiation of the M-intermediates, ^{13}C CP MAS NMR signals of 14- and 20-^{13}C-labeled retinal in the O-intermediate appeared at 115.4 and 16.4 ppm and were assigned to the 13-*trans*, 15-*syn* configuration. The signals due to the N'-intermediate appeared at 115.4 and 23.9 ppm and were assigned to the 13-*cis* configuration, and were in an equilibrium state with the O-intermediate during thermal decay of the M-intermediates at -60 °C. Thus, photo-irradiation NMR studies revealed the photoreaction pathways from the M- to O-intermediates and the equilibrium state between the N'- and O-intermediate. Further, we evaluated the detailed retinal configurations in the O- and N'-intermediates by performing a density functional theory (DFT) chemical shift calculation. The results showed that the N'-intermediate has a 63° twisted retinal state due to the 13-*cis* configuration. The retinal configurations of the O- and N'-intermediates were determined to be 13-*trans*, 15-*syn* and 13-*cis*, respectively, based on the chemical shift values of [20-^{13}C] and

[14-^{13}C] retinal obtained by photo-irradiation solid-state NMR and DFT calculation.

INTRODUCTION

Pharaonis phoborhodopsin (*p*pR), also called sensory rhodopsin II (SRII), is a membrane protein isolated from the halophilic and alkaliphilic archaeal *Natronomonas pharaonis*, which consists of seven-transmembrane α-helices with a vitamin-A aldehyde retinal as a chromophore (1). All-*trans* retinal is predominantly incorporated into the apoprotein of *p*pR. *p*pR functions as a photo receptor protein by forming a 2:2 complex with the cognate two-helix transducer protein *p*HtrII to transmit the photo-signal into the cytoplasm (2–5). The *p*pR/*p*HtrII complex is involved in negative phototaxis through a cyclic photo-reaction pathway called the photo-cycle. *p*pR has an absorbance maximum at 498 nm in the ground (G) state under dark conditions as the initial state. Light absorption transforms *p*pR from the ground state (*p*pR$_G$) to a K(540 nm)-intermediate with an absorbance maximum of 540 nm. This transformation is initiated by *trans*/*cis* photoisomerization of the retinal. The photo-cycle is followed by several intermediates, such as L(498 nm)-, M(390 nm)-, and O(560 nm)-, undergoing thermal relaxation processes. Finally, the O-intermediate thermally returns to the *p*pR$_G$ state (6).

The K-intermediate has a half-life of approximately 1 μs and its retinal is in the 13-*cis*, 15-*anti* configuration. Transformation of the K-intermediate provides the L-intermediate, which has a half-life of approximately 30 μs and a 13-*cis*, 15-*anti* retinal configuration. Subsequently, a proton is removed from the Schiff base (SB) of the L-intermediate, resulting in transformation to the M-intermediate, which has a long half-life of approximately 1.7 s. The M-intermediate has a 13-*cis*, 15-*anti* retinal

configuration with a deprotonated SB (DPSB). Upon reprotonation, the M-intermediate transforms into the O-intermediate with a protonated SB (PSB), which has a half-life of approximately 770 ms and a 13-*trans*, 13-*syn* retinal configuration (4–7). The M- and O-intermediates have long half-lives as compared with the K- and L-intermediates and thus they are known as late-active intermediates.

Important signal transduction processes such as changes in protein structure are induced at the late step in the photo-cycle. These changes likely include the formation of two specific hydrogen bonds, one between Tyr199^{ppR} and Asn74^{pHtrII}, and one between Thr189^{ppR} and Glu43^{pHtrII}/Ser62^{pHtrII}, as observed in the crystal structure of the *p*pR/*p*HtrII complex in the dark state (8), and K and M states (9, 10). Thr204 is another important residue in *p*pR, and plays a role in color tuning and in the photo-cycle kinetics of *p*pR (11). Further observations have shown that Thr204 is indispensable for the negative phototaxis function of the complex (12). There is steric hindrance in the K-intermediate between the C_{14}-H of retinal and Thr204 (13). At the same time, a specific hydrogen bond alteration occurs between Thr204 and Tyr174 in a *p*HtrII-dependent manner (12). Helix movement in *p*pR and outward tilting of helix F during the photo-cycle have been suggested by various groups (14–16) and are believed to be essential steps for the activation of *p*HtrII. However, no helix tilting was observed in the crystal structure of the M-intermediate of the *p*pR/*p*HtrII complex (9). Following tilting of the F-helix in *p*pR, TM2 in *p*HtrII rotates, transferring the signal to the phosphorylation cascade to initiate rotation of the bacterial flagellar motor, resulting in negative phototaxis.

The photo-cycle as described above depends on the photo-isomerization of retinal. The retinal chromophore in *p*pR forms a covalent bond with a perfectly

conserved Lys residue (Lys205) bonded to a Schiff base. Animal rhodopsin (type II rhodopsin) photobleaches, whereas microbial rhodopsin (type I rhodopsin) retains the retinal through the photo-cycle. Therefore, continuous irradiation of *p*pR with green light results in repeated photo-cycles without photo-bleaching and the photo-intermediates can be trapped in a stationary state using type I rhodopsins such as *p*pR (1, 5, 17).

Photo-irradiation solid-state NMR spectroscopy has been used to reveal the photo-activated intermediates of retinal membrane proteins. For example, photo-activated intermediates have been characterized by ^{13}C NMR studies of [^{13}C] retinal and ^{15}N NMR studies of [ζ-^{15}N]Lys of bacteriorhodopsin (bR) (18–21). The light-adapted state and the M- and N-intermediates of bR have been investigated using photo-irradiation solid-state NMR spectroscopy (19, 20). The early M-intermediate, M_0, and late M-intermediate, M_n, in the bR photo-cycle have been characterized by *in-situ* photo-irradiation solid-state NMR spectrometry (22–24). The combination of NMR spectroscopy with a dynamic nuclear polarization (DNP) method revealed the heterogeneity of dark-adapted bR and distortion in the K-intermediate, and four discrete L-intermediates were detected (25, 26). In addition to bR, the photoactive site of channelrhodopsin-2 was revealed (27). Thus, we have developed an *in-situ* photo-irradiation solid-state NMR apparatus that allows irradiation of the sample with extremely high efficiency and enables observation of the photo-intermediates and photoreaction processes of photoreceptor membrane proteins (28–35).

We previously trapped several photo-intermediates in the photo-stationary state using *in-situ* photo-irradiation solid-state NMR and observed the M-intermediates of *p*pR under green light irradiation (29). Continuous irradiation of *p*pR with green light

(520 nm) resulted in the accumulation of late-active intermediates such as multiple M-intermediates (M1, M2 and M3) because of their long life times as compared with the early photo–intermediates such as the K- and L-intermediates. Generally, the half-lives of the late intermediates of sensory-type rhodopsin are much longer than that of ion pump-type rhodopsins such as bR (5). It is reasonable that the longer half-lives time of the photo-intermediates in sensory rhodopsins are accompanied by dynamic conformational changes to allow signal transmission to the transducer protein and signal amplification during the photo-cycle, while the fast photocycle is advantageous for transporting ions during the photocycle of ion pump-type rhodopsins.

In this study, we focus on observing the late photo-intermediates after the M-intermediates by performing *in-situ* photo-irradiation solid-sate NMR measurements using two LED light sources, one each at 520 nm (green light) and 365 nm (blue light). We previously showed that the ^{13}C NMR signal from [20-^{13}C] retinal responds sensitively to changes in the 13C=14C configuration in retinal. Similarly, the ^{13}C NMR signal from [14-^{13}C] retinal should be sensitive to changes in the 15C=Nζ configuration in retinal. Here, we specifically detected the ^{13}C NMR signal from [14, 20-^{13}C] labeled retinal in *p*pR. Based on the chemical shift values for [20-^{13}C] and [14-^{13}C] retinal in the late-active intermediates, and the results of density functional theory (DFT) calculations, we discuss the detailed configurations of these intermediates.

MATERIALS AND METHODS

Sample preparation

[14, 20-^{13}C]-Labeled-retinal-*p*pR with a His-tag (6xHis) at the C-terminal was over-expressed in *Escherichia coli* BL21(DE3) strain in LB medium by induction with

1 mM isopropyl-1-thio-β-D-galactoside (IPTG) and 10 μM [14, 20-^{13}C]-labeled-all-*trans*-retinal. Protein expression was performed at 25°C for 15 hrs. To purify the sample, the cells were lysed by ultra-sonication, then the proteins were solubilized using n-dodecyl-β-D-maltoside (DDM) and purified with Ni-NTA column (QIAGEN, Hilden, Germany) as previously described (29, 36, 37). *p*HtrII(1-159) was also prepared by the same method as described previously (29). After purification, *p*pR was mixed with *p*HtrII at a 1:1 molar ratio by electrophoresis and by monitoring UV-vis absorption and thermal stability (38) of the *p*pR/*p*HtrII complex. The complex was reconstituted into membrane, using DDM micelles incorporating a lipid film of L-α-egg-phosphatidylcholine (egg-PC) (*p*pR:egg-PC molar ratio of 1:30), then DDM was removed by using Bio-Beads (Bio-RAD, Hercules, CA). The reconstituted samples were suspended in 5 mM 2-[4-(2-hydroxyethyl-1-piperazinyl) ethanesulfonic acid (HEPES), 10 mM NaCl buffer solution (pH 7) to provide *p*pR and *p*pR/*p*HtrII complex embedded in egg-PC lipid bilayers.

Solid-state NMR experiments

The fully hydrated sample was concentrated by centrifugation so that the molar ratio of water : lipid : protein was reached to 8350 : 30 : 1 with the hydrated ratio of 300 %. Consequently, 66 mg of hydrated sample with 9 mg of protein was packed into a 5.0 mm outer diameter (o.d.) zirconia pencil-type rotor with a tightly sealed glass cap. Solid-state NMR experiments were performed on a CMX-400 Infinity (Chemagnetics, Fort Collins, CO) solid state NMR spectrometer equipped with an *in-situ* photo-irradiation NMR system using resonance frequencies of 400 and 100 MHz for ^{1}H and ^{13}C nuclei, respectively. ^{13}C cross-polarization magic-angle spinning (CP-MAS)

experiments (39) were performed using the following conditions: ^{13}C 90º pulse of 5.4 μs, ^{1}H decoupling amplitude of 50 kHz, temperatures of -40 and -60 °C and a MAS frequency of 4.0 kHz. TPPM proton high power decoupling (40) was employed during each acquisition. Typically, 40000 transients were accumulated for about 44 hrs. to obtain each 1D CP MAS NMR spectrum. ^{13}C chemical shifts were referenced to the carbonyl resonance of glycine powder at 176.03 ppm (tetramethylsilane (TMS) at 0.0 ppm).

In-situ photo-irradiation solid-state NMR measurements

In-situ continuous photo-irradiation was carried out using an optical fiber passed from outside the magnet through a tightly sealed glass cap made from a glass rod glued to a zirconia rotor (29, 30, 33). The glass rod was grained so as to provide illumination perpendicular to the rotor wall. The fluid membrane proteins were attached to the side wall of the rotor as a thin film and then light was directed perpendicular to the rotor wall from inside the spinner. If the irradiation is not perpendicular to the rotor wall, the light is completely reflected off the surface of the film sample and does not penetrate into the sample. Use of CMX-400 Infinity NMR spectrometer equipped with this photo-irradiation system allowed us to efficiently irradiate samples in the rotor with green (520 nm) and blue (365 nm) LED light sources.

Stationary trapping of photo-intermediates using *in-situ* photo-irradiation solid-state NMR

In-situ photo-irradiation is particularly useful for studying the photo-cycle of several retinal binding membrane proteins. The half-life of the M-intermediate in *p*pR is

approximately 1.7 s, which is much longer than that of the other intermediates, as shown in Fig. 1(A). Thus, continuous irradiation of a sample with green light (520 nm) (Green) traps the M-intermediates in a stationary fashion as schematically shown in Fig. 1B(b), making it possible to detect relatively short-lived intermediates in the stationary state when their half-life differs from those of other intermediates. After green light is turned off (Dark 2), the M-intermediates relax to the G-state (Figure 1B(c)). Difference spectrum between Green and Dark1 which is observed in the dark condition (Fig. 1B(a)) (Green – Dark1: Fig. 1B(d)) indicates the photo reaction pathway from Dark1 to Green and shows that the G-state is transformed to the M-intermediate. Namely, a negative peak shows the reactant and the positive peak shows the product. Similarly, thermal relaxation process from Green to Dark2 is shown in the difference spectrum subtracting Green from Dark2 (Dark2 – Green; Fig. 1B(e)) which indicates that the M-intermediate is transformed to the G-state.

The trapping efficiency can be increased by decreasing the temperature because the photoreaction is a thermal process except for the photoillumination process (G → K), and therefore lowering the temperature extends the half-life of the M-intermediates. The M-intermediates can be eliminated by illuminating with 365 nm LED light since the M-intermediates have a maximum absorbance frequency of 390 nm, which is different from the absorbance frequencies of the other intermediates. The M-intermediates can therefore be selectively eliminated by directly irradiating with 365 nm blue light, allowing detection of the activation of consecutive photoreaction processes, such as the double-photon process, by illuminating with multiple wavelengths. It is thus possible to select a particular intermediate by adjusting either temperature or wavelength.

Figure 1.

Computing method to evaluate ^{13}C chemical shift values of retinal

^{13}C chemical shifts of backbone Cα, C=O and sidechain Cβ signals are significantly displaced for a variety of amino acid residues in polypeptides and proteins, depending on their local conformation such as α-helix, β-sheet or random coil (41). ^{13}C chemical shifts of [20-^{13}C] retinal are correlated with 13-*cis*/*trans* of 13C=14C configuration and [14-^{13}C] retinal are correlated with 15-*syn*/*anti* of 15C=Nζ configuration as experimentally obtained from various retinal proteins and summarized in Table S1. Here, we calculate the ^{13}C chemical shift values of retinal carbons to elucidate the relation between the ^{13}C chemical shift values and retinal configuration.

The ^{13}C chemical shift calculations were performed using the GIAO method (42–46) in the Gaussian09 (47) program with the B3LYP/6-311+g** theory/basis set combination. The calculated chemical shifts were converted to ppm relative to TMS. A schematic structure of retinal, used in the chemical shift calculation, is shown in Fig. 2. Retinal binds to the protein through the side chain of Lys 205, as shown in Fig. 2. The Schiff base was considered to be protonated in the calculation. The initial structure of the retinal was in the all-*trans* configuration of the crystal structure (pdb ID:1JGJ) (48), which corresponds to the G state configuration. We investigated the configurations of the O- and N'-intermediates by evaluating the dependence of the ^{13}C NMR chemical shift on the configuration of retinal according to the rotation of the dihedral angles of 12C-13C=14C-15C, 14C-15C=Nζ-Cε, and 15C=Nζ-Cε-Cδ, abbreviated Φ, Ψ, and X, respectively (Fig. 2). The geometries of the heavy atoms of retinal were fixed in each

dihedral angle and only the hydrogen atoms were optimized with the same theory/basis set conditions before calculation of the chemical shift values. The basis set dependence of the calculation of chemical shift was examined for G-state of retinal using several basis sets. The results were shown in Table S2. It showed that the calculated values are almost the same as those in these large basis sets. In this work, the largest basis set of 6-311+G** in the table was used in all the calculation.

Figure 2

RESULTS AND DISCUSSION

Photoreaction pathways under green light irradiation of the *p*pR/*p*HtrII complex

In-situ photo-irradiation solid-state ^{13}C CP-MAS measurements were performed on the [20-^{13}C]-labeled-retinal-*p*pR/*p*HtrII complex at -40 ºC. We obtained the photoreaction pathways under illumination with green light by first observing the ^{13}C CP-MAS NMR spectrum of the *p*pR/*p*HtrII complex in the dark condition (Dark1) at -40 ºC (Fig. 3A(a) and Figure S1A(a) for full spectrum) and then the ^{13}C CP-MAS spectrum under illumination with 520 nm green light (Fig. 3A(b) and Fig. S1A(b) for full spectrum) to observe the intermediates in stationary state.

The [20-^{13}C] retinal signals shown in Fig. 3A(a) and A(b) heavily overlapped with the lipid signals. The difference spectrum (Green – Dark1) was therefore obtained as shown in Fig. 3A(d), and Fig. S1A(d) for full spectrum to analyze the photoreaction pathways induced by photo-irradiation. The difference spectrum between the light and dark states indicated that the negative peaks correspond to the reactant state and the positive peaks correspond to the product state. Thus, the ^{13}C CP-MAS NMR signal of

the G-state at 13.5 ppm decreased and those of the M-intermediates at 22.1 ppm and 22.9 ppm (M1 and M2), the N'-intermediate at 23.9 ppm and the O-intermediate at 16.1 ppm, all increased. We discuss the assignment of the N'- and O-intermediates in a later section. The ^{13}C CP-MAS NMR signals of the [20-^{13}C] retinal-*p*pR/*p*HtrII complex show the process of transforming from the G-state (13.5 ppm) to a number of photo-intermediates. We previously reported that the G-state was transformed to three kinds of M-intermediates (M1, M2, M3) upon illumination with green light at -20 ºC (29). In the present experiment, at -40º C, we observed photo-intermediates in the 13-*cis* form (22.9, 22.1, and 23.8 ppm) which were assigned to M1, M2, and N'-intermediate, respectively. The signal at 23.8 ppm was previously assigned to M3-intermediate. The photo-intermediate in the 13-*trans* form (16.1 ppm) was assigned to the O-intermediate. In summary, the 13-*trans* form product peak at 16.1 ppm can be assigned to the O-intermediate and the 13-*cis* form can be assigned to the M-intermediates (22.1, 22.9 ppm) and the N'-intermediate (23.9 ppm), as discussed below. The chemical shift values are summarized in Table 1.

Figure 3

Table 1

Relaxation process from the green light irradiation state (Green) to the short dark state (Dark2)

The green light irradiation state was relaxed to the dark state by the process of thermal relaxation. Fig. 3A(c) and Fig. S1A(c) for full spectrum shows the ^{13}C CP-MAS

NMR spectrum of *p*pR/*p*HtrII complex obtained one day after terminating green light irradiation. The difference spectrum shown in Fig. 3B(e) and Fig. S1A(e) for full spectrum was obtained by subtracting the initial dark state (Dark1) from the second short dark state (Dark2). The peak at 23.9 ppm remained unchanged while the peaks at 22.1 and 22.9 ppm decreased in intensity. The difference spectrum shown in Fig. 3B(f) and Fig. S1A(f) for full spectrum was obtained by subtracting the green light illumination state (green) from the second short dark state (Dark2). The peaks at 22.1, 22.9 and 16.1 ppm decreased and the G-state increased in intensity. These results indicate that the peak at 23.9 ppm is not due to the M-intermediates but rather to the N'-intermediate, and therefore the half-lives of the M-intermediates at 22.1 and 22.9 ppm and of the O-intermediate at 16.1 ppm are much shorter than that of the N'-intermediate at 23.9 ppm. Therefore, we conclude that the M- and O-intermediates relaxed to the G-state, and the N'-intermediate relaxed more slowly than the M- and O-intermediates.

Photoreaction pathway from the M-intermediates to the O-intermediate

A N-like intermediate with an absorbance maximum at 500 nm was previously observed in *pharaonis* phobohodopsin in the 13-*cis* form in a transient absorption study (49) that used azide to accelerate the decay of the M-intermediates (50). To confirm the existence of this N-like-intermediate, the sample in the present study was irradiated with near-UV (blue) light at 365 nm to eliminate the M-intermediates (51), which have a maximum absorbance of 390 nm, after the accumulation of photo-intermediates by irradiation with 520 nm light.

Irradiation of the *p*pR/*p*HtrII complex with 520 nm green light at -40 ºC

converted the G-state to the O-, M- and N'-intermediates (Fig. 3B(d) and Fig. 4A(a)). We found that the signal at 23.9 ppm did not decay upon irradiation with 365 nm light (Fig. 4A(b)). As described above, M-intermediates have an absorbance maximum at 390 nm due to the deprotonated Schiff base. Therefore, M-intermediates immediately decay upon illumination with 365 nm blue light (51) and thus the remaining signal corresponding to the 13-*cis* form is assigned to the N'-intermediate (23.9 ppm).

After the M-intermediates of the *p*pR/*p*HtrII complex were trapped at -40 ºC in a stationary manner by illumination with green light (Fig. 4A(a)), irradiation with LED light at 520 nm was switched to 365 nm (Fig. 4A(b)). During this process, the intensities of the M-intermediates decayed while the intensities of the O-intermediate and the G-state increased (Fig. 4A(c)), whereas the N'-intermediate did not decay over the same period (Fig. 4A(b)). Furthermore, it is noted that the M-intermediates were transformed to the O-intermediate following irradiation with 365 nm blue light (Fig. 4A(c)). The M-intermediates are reportedly transformed back to the G-state by irradiation with blue light (365 nm) (51), since the M-intermediates have a maximum absorption of 390 nm. However, it was found in this experiment that the M-intermediates are transformed to the O-intermediate upon irradiation with 365 nm blue light (Fig. 4A(c)). As described above, spectroscopic evidence for the formation of an N'-intermediate was recently obtained in a transient absorption study (50), which reported that decay of the M-intermediates does not directly produce the N'-intermediate but rather produces an O-intermediate that is in equilibrium with the N'-intermediate. Based on previously reported finding and the results of the present *in-situ* photo-irradiation solid-state NMR experiments, we summarize the photoreaction cycle of the *p*pR/*p*HtrII complex as follows (Fig. 5). The M-intermediates are converted

to the O-intermediate under irradiation with 365 nm blue light through a double-photon process, and the O-intermediate is then converted to the N'-intermediate until an equilibrium state is achieved in which the intensity of the N'-intermediate is higher than that of the O-intermediate (Fig. 4A(b)).

It has been reported that M-intermediate is converted to *p*pR'-intermediate at low temperature of -160 ºC under near UV-light irradiation and then back to *p*pR-state (52). This kind of *p*pR'-intermediate was not possibly accumulated at -40 and -60 ºC in the present experiment. Moreover, it is not ruled out the possibility that ^{13}C NMR signals of *p*pR'-intermediate are completely overlapped with those of *p*pR and thus *p*pR'-intermediate is not identified in this experiment

Double-photon process from the G-state to the O-intermediate

We identified the transformation process from the G-state to the O-intermediate by observing the difference in the ^{13}C CP-MAS spectrum upon the blue light (365 nm) irradiation of the G-state. The ^{13}C CP-MAS NMR spectral measurement of the [20-^{13}C] retinal-*p*pR/*p*HtrII complex was first performed under initial dark conditions (Dark1) at -40 ºC. Upon switching directly from the initial dark condition (Dark1) to 365 nm blue light illumination, the M-intermediates were converted to the O-intermediate through a double-photon process (Fig. 4B(d)). Consequently, the O-intermediate was converted to the N'-intermediate until an equilibrium state (Fig. 4B(e)). This pathway was clearly observed in the difference spectrum generated by subtracting the blue light (365 nm) illumination state from the Dark2 state (Fig. 4B(f)).

Figure 4

Figure 5

Photo-reaction pathways of *p*pR from the G-state to the M-intermediates at -40°C

We obtained the ^{13}C CP-MAS NMR signals of [20-^{13}C] retinal-*p*pR without *p*HtrII reconstituted in egg-PC under the initial dark conditions (Fig. 6A(a)) followed by green light illumination with a 520 nm LED (Fig. 6A(b)). The difference spectrum (Fig. 6A(c)) between the M-intermediates and the G-state (Fig. 6A(a) - A(b)) indicated the transformation process from the G-state to the M-intermediate.

The ^{13}C CP-MAS NMR spectra of [20-^{13}C] retinal-*p*pR under the green light illumination with a 520 nm LED (Fig. 6B(d)) and in the subsequent dark condition (Dark2) (Fig. 6B(e)), and the difference spectrum (Fig. 6B(f)) between the dark2 condition and the green light condition (Fig. 6B(e) - B(d)), indicated that the M-intermediate transformed to the G-state via a thermal relaxation decay process at -40 °C in *p*pR alone.

The ^{13}C NMR spectra of [14-^{13}C] retinal-*p*pR (Fig. 6C and D) and the difference spectrum also indicated the process G-state → M-intermediate → G-state, as for [20-^{13}C] retinal-*p*pR. In addition, the chemical shift values of [14-^{13}C] retinal-*p*pR were 121.7 ppm (G-state) and 126.8 ppm (M-intermediate) at -40 °C (Table 1).

Figure 6

Photoreaction pathways from the M-intermediate to the O-intermediate in *p*pR

The M-, N'- and O-intermediates were observed under continuous green light (520

nm) illumination at -40 °C using *p*pR/*p*HtrII complex. In contrast to the case of *p*pR/*p*HtrII, in the *p*pR alone, the N'- and O-intermediates could not be trapped at -40 °C, indicating shorter half-lives than those of *p*pR/*p*HtrII complex. As expected, these intermediates were successfully trapped at -60 °C (Fig. 7A(a)).

In-situ photo-irradiation solid-state ^{13}C CP-MAS measurements were performed on [20-^{13}C] retinal-*p*pR alone at -60 ºC. Under illumination with green light, the difference ^{13}C CP-MAS NMR spectrum of [20-^{13}C] retinal-*p*pR (green light illumination (Green) – initial dark condition (Dark1)) indicated the transformation process from the G-sate (13.6 ppm) to the O-, M- and N'-intermediates (16.4, 22.3 and 23.9 ppm) (Fig. 7A (a)). After stationary trapping of these photo-intermediates, the light source was switched from 520 nm to 360 nm. The result indicated that the signal of the M-intermediates (22.6 ppm) decreased and the signal of the O-intermediate (16.4 ppm) increased (Fig. 7A(b)). The absorbance maximum of the M-intermediate was 395 nm and thus this result indicated that the M-intermediates were transformed to the O-intermediate by irradiation with 365 nm blue light (Fig. 7A(c)).

Figure 7

Relaxation process from the O-intermediate to the N'-intermediate.

We obtained the relaxation process from the O-intermediate to the N'-intermediate, from the difference spectra shown in Fig. 7B. The difference ^{13}C CP-MAS NMR spectrum of [20-^{13}C] retinal-*p*pR between the blue (365 nm) state (Blue) and initial dark conditions (Dark1) indicated that the product photo-intermediates were the O- and N'-intermediates in the blue light (365 nm) illumination state. By turning off the

irradiation, the O-intermediate was converted to the N'-intermediate, as with the *p*pR/*p*HtrII complex (Fig. 7B(e)). This pathway was clearly observed in the difference spectrum generated by subtracting the blue light (365 nm) illumination state from the Dark2 state (Fig. 7B(f)).

Chemical shift values of [14-^{13}C] retinal for the intermediates in *p*pR

We revealed the configurations of the O- and N'-intermediate by measuring the ^{13}C CP-MAS NMR spectra of [14-^{13}C] retinal-*p*pR. The chemical shift values of [14-^{13}C] retinal contain important information regarding the 15-*syn*/*anti* configuration (20, 33). The spectra shown in Fig. 8 show the region from 100.0 ppm to 150.0 ppm for the same experiments as shown in Fig. 7 and indicate the chemical shifts of [14-^{13}C] retinal-*p*pR. At -60 °C, *in-situ* photo-irradiation solid-state ^{13}C CP-MAS spectra were observed for [14-^{13}C] retinal-*p*pR and the signal at 127.1 ppm was assigned to [14-^{13}C] retinal in the M-intermediates resulting from a transformation process from the G-sate to the M-intermediates under green light (520 nm) illumination (Fig. 8A(a)). Subsequent blue light (365 nm) illumination resulted in an intense signal from the O-intermediate, as with the signal of [20-^{13}C] retinal-*p*pR shown in Fig. 7. Therefore, the main positive peak in the difference spectrum (Fig. 8A(b)) was assigned to the O-intermediate and the chemical shift value of [14-^{13}C] retinal was 115.4 ppm. As discussed above, the M-intermediates transforms to the O-intermediate upon blue light (365 nm) illumination and thus the chemical shift value at 115.4 ppm was indeed due to the O-intermediate (Fig. 8A(c)). The spectrum shown in Fig. 8B(d) also indicated that the 115.4 ppm signal is assignable to the O-intermediate due to the double photon process from the G-state to the O-intermediate upon blue light (365 nm) illumination.

The difference spectrum shown in Fig. 8B(e) clearly indicated that the 115.4 ppm signal also belonged to the N'-intermediate because the N'-intermediate showed a very long half-life and the signal intensity remained unchanged at -60 °C as shown in Fig. 7(b, e). In addition, the thermal relaxation pathway of the O-intermediate was observed as a decrease in the signal at 115.4 ppm (Fig. 8B(f)).

Figure 8

Conformation of retinal in the late photo-intermediates

We have assigned the ^{13}C NMR chemical shift values for the late photo-intermediates M-, O- and N'-intermediates (Table 1). The configuration of the M-intermediates was clearly shown to be 13-*cis*,15-*anti* by comparing the present result with previous studies of Salinibacter sensory rhodopsin I (SrSRI), bR and its mutant Y185F-bR (20, 30, 33) (Table S1). Furthermore, the deprotonated Schiff base state in the M-intermediates was obtained as a result of the fast transformation process initiated by blue light (365 nm) illumination. This comparison and our previous studies in *p*pR and SrSRI (31, 30) allow the 13C=14C configuration of retinal in the O- and N'-intermediates to be assigned to the 13-*trans* and 13-*cis* forms, respectively. The 15C=Nζ configuration is more challenging because the value of 115.4 ppm is the boundary region between the 15-*syn* and 15-*anti* forms. For example, in the study of Y185F-bR, the CS* intermediate has been assigned to the 15-*syn* form and the chemical shift value of [14-^{13}C] retinal was 115.3 ppm (33). On the other hand, the N-intermediate of wt-bR has been assigned to the 15-*anti* form and the chemical shift value of [14-^{13}C] retinal was 115.2 ppm (53) (Table S1). The following is a detailed

discussion of the configurations of the O- and N'-intermediates as elucidated by DFT calculation.

Determination of the dihedral angles Φ for the O- and N'-intermediates

We elucidated the configuration of the O- and N'-intermediates by investigating the relationship between the ^{13}C NMR chemical shift values and configuration by using DFT calculation. The crystal structure (pdb ID:1JGJ) (48) corresponding to the G state was used as a starting configuration, and has the dihedral angles $\Phi = -177°$, $\Psi = -175°$ and $X = -66°$. The chemical shift values of 20-^{13}C and 14-^{13}C for this configuration were calculated to be 17.5 and 128.1 ppm, respectively, and these values are shown in Table 2. Touw et al. (54) previously calculated the chemical shift at 20-^{13}C for all-*trans*-retinal to be 18.0 ppm (54), which is very similar to the value obtained in this work. However, these calculated values show some discrepancy with the experimental values, of 13.6 and 121.6 ppm, with the calculated chemical shift values being 3.9 and 6.5 ppm larger than the experimental 20-^{13}C and 14-^{13}C values, respectively. Touw et al. (54) also showed a similar discrepancy. Therefore, in the following discussion, the calculated values will be discussed with corrected values by adding 3.9 and 6.5 ppm to the experimental values for 20-^{13}C and 14-^{13}C in retinal, respectively.

The dependence of the chemical shift value of 20-^{13}C in retinal on the dihedral angles Φ and Ψ were investigated and the results are shown in Fig. 9(A) and (B), respectively. The chemical shift at 20-^{13}C in retinal drastically changes according to the rotation of dihedral angle Φ but it is almost independent of the change in the dihedral angle Ψ. These results indicate that the value of 20-^{13}C can be used to determine the

configuration with dihedral angle Φ. The experimental chemical shift values of 20-^{13}C for the O- and N'-intermediates were 16.4 and 23.9 ppm and thus the corrected values of these conformations should be 20.3 and 27.8 ppm, respectively. The positions of these values are shown in Fig. 9(A). The corresponding dihedral angle Φ for the O-intermediate configuration was estimated as -150° and for the N'-intermediate it was estimated as -63°, as shown in Table 2.

Figure 9

Table 2

Determination of the dihedral angle Ψ for the O-intermediate

The dihedral angle Φ in the O-intermediate was estimated to be -150° and thus the dihedral angle Ψ was investigated for this intermediate next. The dependence of the chemical shift value of 14-^{13}C in retinal on the dihedral angle Ψ was evaluated by setting Φ at -150° and X at -66°. The results are shown in Fig. 10 (dashed line) and indicate that the chemical shift value for the 15-*syn* form was larger than that of the 15-*anti* form. However, previous experiments showed the opposite. For example, the values of 14-^{13}C for 15-*anti* and 15-*syn* were 122.0 ppm and 110.5 ppm for bR as shown in Table S1 and thus the calculated chemical shift of the *syn*-state should be up-field compared to that of the *anti*-state.

We resolved this discrepancy by conducting calculations using the *trans* configuration for dihedral angle X (X = -180°) because in this configuration we would expected a γ-effect between the 14-^{13}C proton and the ε proton (55). The results are also

shown in Fig. 10 and indicate that the chemical shift value of 14-^{13}C in the *syn* conformation (Ψ = 0°) changed by -4.0 ppm from anti (Ψ = -180°) configuration (Fig. 10, (dashed line)). This change in chemical shift allowed estimation of the configuration of the O-intermediate. The experimental chemical shift value of 14-^{13}C of the O-intermediate was 115.4 ppm, as summarized in Table 1, and thus the offset value of this configurations should be 121.9 ppm, corresponding to a dihedral angle Ψ of 0°. The configuration of the O-intermediate can thus be determined to have the dihedral angles Φ and Ψ of -150° and 0°, respectively, as listed in Table 2. These results indicated that the configuration of the O-intermediate was, in general, in the 13-*trans* and 15-*syn* form.

Figure 10

Determination of the dihedral angle Ψ for the N'-intermediate

The dihedral angle of Ψ was estimated in a manner similar to that discussed above. The conformation of the N'-intermediate was calculated using the dependence of the chemical shift value of 14-^{13}C in retinal on the dihedral angle Ψ and the results are shown in Fig. 11. The dihedral angle Φ in the N'-intermediate was set at -63° as estimated in Fig. 9(A). Two sets of values were used in the calculations for the dihedral angle X: the crystal value of -66° and the *trans* form value of -180°, and both the results are shown in Fig. 11. The curves of the chemical shifts allowed estimation of the conformation of the N'-intermediate. The chemical shift value of 14-^{13}C of the N'-intermediate was 115.4 ppm, as summarized in Table 1, and thus the offset value of this conformation should be 121.9 ppm. However, three points correspond to the dihedral

angle Ψ in Fig. 11: the dihedral angles Ψ and X are (Ψ = -175° and X = -66°), (Ψ = -175° and X = -180°), and (Ψ = -17° and X = -180°). Although the dihedral angle Φ in the N'-intermediate was determined as -63°, the remaining dihedral angles Ψ and X could be any of these three possibilities.

Figure 11

CONCLUSION

It is demonstrated that *in-situ* photo-irradiation solid-state NMR spectroscopy allows us to stationary observe photo-intermediates and photo reaction pathways of photo receptor membrane protein such as *p*pR/*p*HtrII complex system to gain insight into the signal transduction mechanism.

We observed the M-, O- and N'-intermediates from *p*pR and *p*pR/*p*HtrII complex reconstituted in egg-PC membrane by irradiation with green light using *in-situ* photo-irradiation solid-state NMR. Changes in the ^{13}C CP-MAS NMR signals resulting from switching the wavelength of light used for continuous irradiation from green light (520 nm) to blue light (365 nm) revealed the pathways of the late photo-active intermediates from the M-intermediates to the O-intermediate. Interestingly, one of the multiple M-intermediates previously reported was identified as an N-like-intermediate reported in bR which we designated the N'-intermediate. The N'-intermediate is produced from the O-intermediate in *p*pR, while the N-intermediate is produced from M-intermediate in bR. This result indicates that large structural changes of the proteins is necessary to produce the N'-intermediate which is in an equilibrium state with the O-intermediate. In addition, half-life of the N'-intermediate for ppR/pHtrII complex

showed longer than that for *p*pR. In the physiological point of view, we suggested that the N'-intermediate might play important role in signaling processes as a pre-amplitude mechanism because it has a long half-life and is in equilibrium with the O-intermediate. Detailed configurations of the O- and N'-intermediates were revealed to be 13-*trans*, 15-*syn* and 13-*cis*, respectively, by NMR experiments and DFT calculation and showed that the chemical shift values of [14-^{13}C] retinal are useful for determining the 15-*syn* or 15- *anti* configuration. The results of our DFT calculation are the first step of the trial to find the conformation of the intermediate states of the retinal which would be difficult to get only from the experimental work. Further refinement of the calculation will be needed to confirm the proposed intermediate conformations in future.

SUPPORTING MATERIAL

Supporting Materials, two tables and one figure are available at http://www.biophys.org/

AUTHOTR CONTRIBUTIONS

M.Y., performed NMR measurements, DFT calculation and analyses, and wrote the article. I.K., and A.N designed NMR experiments and wrote the article. K.U. performed DFT calculation and wrote the article. T.O., and A.W. prepared labeled retinal. K.N. and Y.S. designed sample preparation and gave valuable discussion on the article.

ACKNOWLEDGMENTS

This work was supported by Grants-in-Aid for Scientific Research in an Innovative Area (16H00756 to AN, 25104005 to YS and 16H00828 to IK), and by a Grant-in-Aid for Scientific Research (C) (15K06963 to AN) and Research (B)

(15H04363 to YS and 15H04336 to IK) and a Grant-in-Aid for JSPS Research Fellow (16J00073 to YM) from the Ministry of Culture, Sports, Science and Technology of Japan. This work was also supported by JST-CREST and AMED grant to YS. The authors thank the Research Center for Computational Science, Okazaki, Japan, for use of their computing facilities to perform a part of the calculation described in this paper.

REFERENCES

1. Govorunova, E.G., O.A. Sineshchekov, H. Li, and J.L. Spudich. 2017. Microbial Rhodopsins: Diversity, Mechanisms, and Optogenetic Applications. Annu Rev Biochem. 86: 845–872.
2. Hoff, W.D., K.-H. Jung, and J.L. Spudich. 1997. Molecular mechanism of photosignaling by archaeal sensory rhodopsins. Annu. Rev. Biophys. Biomol. Struct. 26: 223–258.
3. Spudich, J.L., and H. Luecke. 2002. Sensory rhodopsin II: functional insights from structure. Curr. Opin. Struct. Biol. 12: 540–546.
4. Suzuki, D., H. Irieda, M. Homma, I. Kawagishi, and Y. Sudo. 2010. Phototactic and chemotactic signal transduction by transmembrane receptors and transducers in microorganisms. Sensors. 10: 4010–4039.
5. Inoue, K., T. Tsukamoto, and Y. Sudo. 2014. Molecular and evolutionary aspects of microbial sensory rhodopsins. Biochim. Biophys. Acta - Bioenerg. 1837: 562–577.
6. Kamo, N., K. Shimono, M. Iwamoto, and Y. Sudo. 2001. Photochemistry and Photoinduced Proton Transfer by Pharaonis Phoborhodopsin. Biochem. 66: 1277–1282.
7. Imamoto, Y., Y. Shichida, J. Hirayama, H. Tomioka, N. Kamo, and T. Yoshizawa. 1992. Chromophore Configuration of Pharaonis Phoborhodopsin and Its Isomerization on Photon Absorption. Biochemistry. 31: 2523–2528.
8. Gordeliy, V.I., J. Labahn, R. Moukhametzianov, R. Efremov, J. Granzin, R. Schlesinger, G. Büldt, T. Savopol, A.J. Scheidig, J.P. Klare, and M. Engelhard. 2002. Molecular basis of transmembrane signalling by sensory rhodopsin

II-transducer complex. Nature. 419: 484–487.

9. Moukhametzianov, R., J.P. Klare, R. Efremov, C. Baeken, A. Göppner, J. Labahn, M. Engelhard, G. Büldt, and V.I. Gordeliy. 2006. Development of the signal in sensory rhodopsin and its transfer to the cognate transducer. Nature. 440: 115–119.

10. Ishchenko, A., E. Round, V. Borshchevskiy, S. Grudinin, I. Gushchin, and J.P. Klare, A. Remeeve, V. Polovinkin, P. Utrobin, T. Balandin, M. Engelhard, G. Büldt, and V. Gordeliy. 2017. New Insights on Signal Propagation by Sensory Rhodopsin II / Transducer Complex. Sci. Rep. 7: 41811.

11. Shimono, K., T. Hayashi, Y. Ikeura, Y. Sudo, M. Iwamoto, and N. Kamo. 2003. Importance of the broad regional interaction for spectral Tuning in natronobacterium pharaonis phoborhodopsin (sensory rhodopsin II). J. Biol. Chem. 278: 23882–23889.

12. Sudo, Y., Y. Furutani, H. Kandori, and J.L. Spudich. 2006. Functional importance of the interhelical hydrogen bond between Thr ^{204} and Tyr^{174} of sensory rhodopsin II and its alteration during the signaling process. J. Biol. Chem. 281: 34239–34245.

13. Sudo, Y., Y. Furutani, A. Wada, M. Ito, N. Kamo, and H. Kandori. 2005. Steric constraint in the primary photoproduct of an archaeal rhodopsin from regiospecific perturbation of C-D stretching vibration of the retinyl chromophore. J. Am. Chem. Soc. 127: 16036–16037.

14. Wegener, A.A., I. Chizhov, M. Engelhard, and H.J. Steinhoff. 2000. Time-resolved detection of transient movement of helix F in spin-labelled pharaonis sensory rhodopsin II. J. Mol. Biol. 301: 881–891.

15. Spudich, J.L. 1998. Variations on a molecular switch: Transport and sensory signalling by archaeal rhodopsins. Mol. Microbiol. 28: 1051–1058.

16. Yoshida, H., Y. Sudo, K. Shimono, M. Iwamotoa, and N. Kamo. 2004. Transient movement of helix F revealed by photo-induced inactivation by reaction of a bulky SH-reagent to cysteine-introduced pharaonis phoborhodopsin (sensory rhodopsin II). Photochem. Photobiol. Sci. 3: 537–542.

17. Ernst, O.P., D.T. Lodowski, M. Elstner, P. Hegemann, L.S. Brown, and H. Kandori. 2014. Microbial and Animal Rhodopsins : Structures, Functions and Molecular Mechanisms. Chem. Rev. 114: 126–163.

18. Smith, S.O., H.J.M. de Groot, R. Gebhard, J.M.L. Courtin, J. Lugtenburg, J. Herzfeld, and R.G. Griffin. 1989. Structure and Protein Environment of the Retinal Chromophore in Light- and Dark-Adapted Bacteriorhodopsin Studied by Solid-State NMR. Biochemistry. 28: 8897–8904.

19. McDermott, A.E., L.K. Thompson, C. Winkel, M.R. Farrar, S. Pelletier, J. Lugtenburg, J. Herzfeld, and R.G. Griffin. 1991. Mechanism of Proton Pumping in Bacteriorhodopsin by Solid-State NMR: The Protonation State of Tyrosine in the Light-Adapted and M States. Biochemistry. 30: 8366–8371.

20. Farrar, M.R., K. V. Lakshmi, S.O. Smith, R.S. Brown, J. Raap, J. Lugtenburg, R.G. Griffin, and J. Herzfeld. 1993. Solid state NMR study of [ε-^{13}C]Lys-bacteriorhodopsin: Schiff base photoisomerization. Biophys. J. 65: 310–315.

21. de Groot, H.J.M., S.O. Smith, J. Courtin, E. van den Berg, C. Winkel, J. Lugtenburg, R.G. Griffin, and J. Herzfeld. 1990. Solid-state ^{13}C and ^{15}N NMR study of the low pH forms of bacteriorhodopsin. Biochemistry. 29: 6873–6883.

22. Hu, J.G., B.Q. Sun, M. Bizounok, M.E. Hatcher, J.C. Lansing, J. Raap, P.J.E. Verdegem, J. Lugtenburg, R.G. Griffin, and J. Herzfeld. 1998. Early and late M intermediates in the bacteriorhodopsin photocycle: A solid-state NMR study. Biochemistry. 37: 8088–8096.

23. Petkova, A.T., M. Hatanaka, C.P. Jaroniec, J.G. Hu, M. Belenky, M. Verhoeven, J. Lugtenburg, R.G. Griffin, and J. Herzfeld. 2002. Tryptophan interactions in bacteriorhodopsin: A heteronuclear solid-state NMR study. Biochemistry. 41: 2429–2437.

24. Hu, J.G., B.Q. Sun, A.T. Petkova, R.G. Griffin, and J. Herzfeld. 1997. The predischarge chromophore in bacteriorhodopsin: A ^{15} N solid-state NMR study of the L photointermediate. Biochemistry. 36: 9316–9322.

25. Mak-Jurkauskas, M.L., V.S. Bajaj, M.K. Hornstein, M. Belenky, R.G. Griffin, and J. Herzfeld. 2008. Energy transformations early in the bacteriorhodopsin photocycle revealed by DNP-enhanced solid-state NMR. Proc. Natl. Acad. Sci. 105: 883–888.

26. Bajaj, V.S., M.L. Mak-Jurkauskas, M. Belenky, J. Herzfeld, and R.G. Griffin. 2009. Functional and shunt states of bacteriorhodopsin resolved by 250 GHz dynamic nuclear polarization-enhanced solid-state NMR. Proc. Natl. Acad. Sci. 106: 9244–9.

27. Becker-Baldus, J., C. Bamann, K. Saxena, H. Gustmann, L.J. Brown, R.C.D. Brown, C. Reiter, E. Bamberg, J. Wachtveitl, H. Schwalbe, and C. Glaubitz. 2015. Enlightening the photoactive site of channelrhodopsin-2 by DNP-enhanced solid-state NMR spectroscopy. Proc. Natl. Acad. Sci. 112: 9896–9901.

28. Kawamura, I., N. Kihara, M. Ohmine, K. Nishimura, S. Tuzi, H. Saitô, and A.

Naito. 2007. Solid-state NMR studies of two backbone conformations at Tyr185 as a function of retinal configurations in the dark, light, and pressure adapted bacteriorhodopsins. J. Am. Chem. Soc. 129: 1016–1017.

29. Tomonaga, Y., T. Hidaka, I. Kawamura, T. Nishio, K. Ohsawa, T. Okitsu, A. Wada, Y. Sudo, N. Kamo, A. Ramamoorthy, and A. Naito. 2011. An active photoreceptor intermediate revealed by in situ photoirradiated solid-state NMR spectroscopy. Biophys. J. 101: L50–L52.

30. Yomoda, H., Y. Makino, Y. Tomonaga, T. Hidaka, I. Kawamura, T. Okitsu, A. Wada, Y. Sudo, and A. Naito. 2014. Color-discriminating retinal configurations of sensory rhodopsin I by photo-irradiation solid-state NMR spectroscopy. Angew. Chemie Int. Ed. 53: 6960–6964.

31. Naito, A., and I. Kawamura. 2014. Photoactivated structural changes in photoreceptor membrane proteins as revealed by in situ photoirradiation solid-state NMR spectroscopy. In: Frances Separovic, A Naito, editors. Advances in Biological Solid-State NMR: Proteins and Membrane-Active Peptides. Cambridge, UK: Royal Society of Chemistry. pp. 387–404.

32. Naito, A., I. Kawamura, and N. Javkhlantugs. 2015. Recent solid-state NMR studies of membrane-bound peptides and proteins. Annu. Reports NMR Spectrosc. 86: 334–411.

33. Oshima, K., A. Shigeta, Y. Makino, I. Kawamura, T. Okitsu, A. Wada, S. Tuzi, T. Iwasa, and A. Naito. 2015. Characterization of photo-intermediates in the photo-reaction pathways of a bacteriorhodopsin Y185F mutant using in situ photo-irradiation solid-state NMR spectroscopy. Photochem. Photobiol. Sci. 14: 1694–1702.

34. Naito, A., Y. Makino, Y. Tasei, and I. Kawamura. 2018. Photoirradiatiion and microwave irradiation NMR spectroscopy . In: the Nuclear Magnetic Resonance Society of Japan, editor. Experimental Approaches of NMR Spectroscopy. Singapore: Springer. pp. 135–170.

35. Naito, A., Y. Makino, and I. Kawamura. 2017. In-Situ Photo Irradiation Solid-State NMR Spectroscopy Applied to Retinal-Binding Membrane Proteins. In: Graham A. Webb, editor. Modern Magnetic Resonance. Springer. pp. 1–22.

36. Kitajima-Ihara, T., Y. Furutani, D. Suzuki, K. Ihara, H. Kandori, M. Homma, and Y. Sudo. 2008. Salinibacter sensory rhodopsin: Sensory rhodopsin I-like protein from a eubacterium. J. Biol. Chem. 283: 23533–23541.

37. Kawamura, I., H. Yoshida, Y. Ikeda, S. Yamaguchi, S. Tuzi, H. Saitô, N. Kamo, and A. Naito. 2008. Dynamics change of phoborhodopsin and transducer by activation: Study Using D75N Mutant of the Receptor by Site-directed Solid-state ^{13}C NMR. Photochem. Photobiol. 84: 921–930.

38. Sudo, Y., M. Yamabi, M. Iwamoto, K. Shimono, and N. Kamo. 2003. Interaction of Natronobacterium pharaonis phoborhodopsin (sensory rhodopsin II) with its cognate transducer probed by increase in the thermal stability. Photochem. Photobiol. 78: 511–6.

39. Schaefer, J., and E.O. Stejskal. 1976. Carbon-13 Nuclear Magnetic Resonance of Polymers Spinning at the Magic Angle. J. Am. Chem. Soc. 98: 1031–1032.

40. Bennett, A.E., C.M. Rienstra, M. Auger, K. V. Lakshmi, and R.G. Griffin. 1995. Heteronuclear decoupling in rotating solids. J. Chem. Phys. 103: 6951–6958.

41. Saitô, H., I. Ando, and A. Ramamoorthy. 2010. Chemical Shift Tensor – the Heart of NMR: Insights into Biological Aspects of Proteins. Prog Nucl Magn

Reson Spectrosc. 57: 181–228.

42. F. London. 1937. Théorie quantique des courants interatomiques dans les combinaisons aromatiques. J. Phys. Le Radium. 8: 397–409.

43. R. Ditchfield. 1972. Molecular Orbital Theory of Magnetic Shielding and Magnetic Susceptibility. J. Chem. Phys. 56: 5688.

44. Ditchfield, R. 1974. Self-consistent perturbation theory of diamagnetism I. A gauge-invariant LCAO method for N.M.R. Chemical shifts. Mol. Phys. 27: 789–807.

45. Woliński, K., and A.J. Sadlej. 1980. Self-consistent perturbation theory open-shell states in perturbation-dependent non-orthogonal basis sets. Mol. Phys. 41: 1419–1430.

46. Wolinski, K., J.F. Hinton, and P. Pulay. 1990. Efficient Implementation of the Gauge-Independent Atomic Orbital Method for NMR Chemical Shift Calculations. J. Am. Chem. Soc. 112: 8251–8260.

47. Frisch, M.J., G.W. Trucks, H.B. Schlegel, G.E. Scuseria, M.A. Robb, J.R. Cheeseman, J.A. Montgomery, T.V. Jr., K.N. Kudin, J.C. Burant, J.M. Millam, S.S. Iyengar, J. Tomasi, V. Barone, B. Mennucci, M. Cossi, G. Scalmani, N. Rega, G.A. Petersson, H. Nakatsuji, M. Hada, M. Ehara, K. Toyota, R. Fukuda, J. Hasegawa, M. Ishida, T. Nakajima, Y. Honda, O. Kitao, H. Nakai, M. Klene, X. Li, J.E. Knox, H.P. Hratchian, J.B. Cross, V. Bakken, C. Adamo, J. Jaramillo, R. Gomperts, R.E. Stratmann, O. Yazyev, A.J. Austin, R. Cammi, C. Pomelli, J.W. Ochterski, P.Y. Ayala, K. Morokuma, G.A. Voth, P. Salvador, J.J. Dannenberg, V.G. Zakrzewski, S. Dapprich, A.D. Daniels, M.C. Strain, O. Farkas, D.K. Malick, A.D. Rabuck, K. Raghavachari, J.B. Foresman, J. V. Ortiz, Q. Cui, A.G.

Baboul, S. Clifford, J. Cioslowski, B.B. Stefanov, G. Liu, A. Liashenko, P. Piskorz, I. Komaromi, R.L. Martin, D.J. Fox, T. Keith, M.A. Al-Laham, C.Y. Peng, A. Nanayakkara, M. Challacombe, P.M.W. Gill, B. Johnson, W. Chen, M.W. Wong, C. Gonzalez, J.A. Pople, and 2004. Gaussian, Inc., Wallingford CT. 2004. Gaussian 09, Revision A.02. .

48. Luecke, H., B. Schobert, J.K. Lanyi, E.N. Spudich, and J.L. Spudich. 2001. Crystal Structure of Sensory Rhodopsin II at 2.4 Angstroms: Insights into Color Tuning and Transducer Interaction. Science. 293: 1499–1503.

49. Chizhov, I., G. Schmies, R. Seidel, J.R. Sydor, B. Lüttenberg, and M. Engelhard. 1998. The photophobic receptor from Natronobacterium pharaonis: Temperature and pH dependencies of the photocycle of sensory rhodopsin II. Biophys. J. 75: 999–1009.

50. Tateishi, Y., T. Abe, J. Tamogami, Y. Nakao, T. Kikukawa, N. Kamo, and M. Unno. 2011. Spectroscopic evidence for the formation of an N intermediate during the photocycle of sensory rhodopsin II (phoborhodopsin) from natronobacterium pharaonis. Biochemistry. 50: 2135–2143.

51. Roy, S., T. Kikukawa, P. Sharma, and N. Kamo. 2006. All-optical switching in Pharaonis phoborhodopsin protein molecules. IEEE Trans Nanobioscience. 5: 178–187.

52. Balashov, S.P., M. Sumi, and N. Kamo. 2000. The M intermediate of Pharaonis phoborhodopsin is photoactive. Biophys. J. 78: 3150–3159.

53. Lakshmi, K. V., M.R. Farrar, J. Herzfeld, R.G. Griffin, J. Raap, J. Lugtenburg, and R.G. Griffin. 1994. Solid State^{13}C and^{15}N NMR Investigations of the N Intermediate of Bacteriorhodopsin. Biochemistry. 33: 8853–8857.

54. Touw, S.I.E., H.J.M. De Groot, and F. Buda. 2004. DFT calculations of the ^{1}H chemical shifts and ^{13}C chemical shift tensors of retinal isomers. J. Mol. Struct. THEOCHEM. 711: 141–147.

55. Harbison, G.S., S.O. Smith, J.A. Pardoen, C. Winkel, J. Lugtenburg, J. Herzfeld, R. Mathies, and R.G. Griffin. 1984. Dark-adapted bacteriorhodopsin contains 13-cis, 15-syn and all-trans, 15-anti retinal Schiff bases. Proc. Natl. Acad. Sci. 81: 1706–1709.

Tables

Table 1 ^{13}C chemical shift values of retinal obtained from NMR experiments

		chemical shift [ppm]		Configuration
		20-^{13}C	14-^{13}C	
*p*pR/*p*HtrII(-40°C)	G-state	13.5±0.8		13-*trans*, 15-*anti*
	O-intermediate	16.1±1.1		13-*trans*
	M-intermediate	22.1, 22.9±1.2		13-*cis*, 15-*anti*
	N'-intermediate	23.9±0.9		13-*cis*
*p*pR (-40°C)	G-state	13.5±0.7	121.7±0.5	13-*trans*, 15-*anti*
	M-intermediate	22.3±1.3	126.8±1.1	13-*cis*, 15-*anti*
*p*pR(-60°C)	G-state	13.6±1.5	121.6±1.7	13-*trans*, 15-*anti*
	O-intermediate	16.4±1.3	115.4±1.8	13-*trans*
	M-intermediate	22.6±1.2	127.1±1.7	13-*cis*, 15-*anti*
	N'-intermediate	23.9±1.5	115.4±1.2	13-*cis*

Table 2 ^{13}C chemical shift values of retinal calculated by DFT, and the conformation of retinal in several photo-intermediates.

	Chemical shift [ppm]		Dihedral angle [degree]			Configuration
	20-^{13}C	14-^{13}C	Φ	Ψ	χ	
G-state	17.5	128.1	-177[a]	-175 [a]	-66 [a]	13-*trans*, 15-*anti*
O-intermediate	20.3	121.9	-150	0	-180	13-*trans*, 15-*syn*
N'-intermediate	27.8	121.9	-63	-175	-180	13-*cis*, 15-*anti*
				-7	-180	13-*cis*, 15-*syn*
				-175	-66[a]	13-*cis*, 15-*anti*

[a]Ref. (48) (pdb ID:1JGJ)

Figure Legends

FIGURE 1. A. Typical photo-cycle of the *p*pR/*p*HtrII complex. The M- and O-intermediates have much longer half-lives than the K- and L-intermediates. B. Schematic experimental protocol and analysis strategy. First, *in-situ* photo-irradiation solid-state NMR spectrum of the G-state was observed in the dark state (Dark1) (B(a)), then the spectrum of the M-intermediate under illumination with green light (Green) (B(b)), and finally in the second dark state (dark2) (B(c)) in which the M-intermediate decreases and the G-state increases. We analyzed the photoreaction pathway and eliminated overlapping signals by obtaining the difference spectra. The difference spectra shown are: B(d) = (b) – (a) showing that the G-state is transformed to the M-intermediate; B(e) = (c) – (b) showing that the M-intermediate is transformed to the G-state; B(f) = (c) – (a) showing that the the G-state is transformed to the M-intermediate. A negative peak in a difference spectrum indicates the reactant and a positive peak indicates a product.

FIGURE 2. Schematic structure of retinal covalently bonded through a Schiff base. The letters α, β, γ, δ, ε are the positions of the carbons of Lys205 in *p*pR. Circled numbers are the positions of carbons observed by ^{13}C CP-MAS solid-state NMR. The dihedral angles Φ, Ψ and X are defined as 12C-13C=14C-15C, 14C-15C=Nζ-Cε, and 15C=Nζ-Cε-Cδ, respectively.

FIGURE 3. A. ^{13}C CP-MAS NMR spectra of the [20-^{13}C] retinal–*p*pR/*p*HtrII complex at -40 ºC using a 4 kHz MAS frequency, (a) acquired under initial dark conditions (Dark1), (b) acquired under irradiation with green light (520 nm) (Green) and (c) obtained one day after turning off irradiation (dark2). B. The difference spectra obtained by (d) Green – Dark1 (process from Dark1 to Green), (e) Dark2 – Dark1 (process from Dark1 to Dark 2) and (f) Dark2 – Green (process from Green to Dark2).

FIGURE 4. ^{13}C CP-MAS NMR difference spectra of the [20-^{13}C] retinal labeled *p*pR/*p*HtrII complex were measured at -40 °C using 4 kHz MAS. A. (a) The difference spectrum obtained by subtracting the initial dark conditions (Dark1) from the green light (520 nm) illumination state (Green) (Green – Dark1). (b) The difference spectrum obtained by subtracting the initial dark conditions (Dark1) from the blue light (365 nm) illumination state (Blue) after the green light stationary state Blue – Dark1. (c) The

difference spectra obtained by Blue – Green, which is identical to (b) – (a). B. (d) The difference spectrum obtained by subtracting Dark1 from Blue (Blue – Dark1). (e) The difference spectrum obtained by subtracting the Dark1 from the second dark condition (Dark2) after turning off irradiation (Dark2 – Dark1). (f) The difference spectra obtained by subtracting Blue from Dark2 (Dark2 – Blue), which is identical to (e) – (d).

FIGURE 5. The photo reaction pathway of *p*pR including the N'-intermediate, as revealed by *in-situ* photo-irradiation solid-state NMR measurements. The O-intermediate is in an equilibrium state with the N'-intermediate. The λ maximum of the N'-intermediate was estimated at 500 nm (50). The transition process from the M-intermediates to the O-intermediate is shown by a blue arrow. The pathway for thermal relaxation from the M-intermediates to the N'-intermediate, and subsequently from the N'-intermediate to the G-state, remain unclear and thus are designated with a black dashed arrow. The general configurations of the O- and N'-intermediates were the 13-*trans*, 15-*syn*, and the 13-*cis* forms, respectively.

FIGURE 6. ^{13}C CP-MAS NMR spectra of [20-^{13}C, 14-^{13}C] retinal-*p*pR without *p*HtrII at -40 °C under 4 kHz MAS. A. The ^{13}C NMR spectra of [20-^{13}C] retinal-*p*pR indicated the transformation process from the G-state (13.5 ppm) to the M-intermediate (22.3 ppm), (a) acquired under initial dark conditions (Dark1), (b) acquired under green light (520 nm) illumination states (Green), and (c) the difference spectrum obtained by subtracting (Dark1) from (Green) (Green – Dark1). B. ^{13}C NMR spectra of [20-^{13}C] retinal-*p*pR showing the thermal relaxation process from the M-intermediate to the G-state, (d) acquired under green light illumination states (Green), (e) acquired under short dark conditions (Dark2) after turning off irradiation, and (f) the difference spectrum obtained by (Green) from (Dark2) (Dark2 – Green). C. ^{13}C NMR spectra showing the region from 100.0 ppm to 150.0 ppm for the same experiment as A, (g) acquired under initial dark conditions (Dark1), (h) acquired under green light illumination states (Green), and (i) the difference spectrum obtained by subtracting the (Dark1) from (Green) (Green – Dark1). D. ^{3}C NMR spectra showing the region from 100.0 ppm to 150.0 ppm for the same experiment as B, (j) acquired under green light illumination states (Green), (k) acquired under short dark conditions (Dark2) after turning off irradiation, and (l) the difference spectrum obtained by subtracting (Green) from (Dark2) (Dark2 – Green). The spectra shown in C and D indicate the transformation process from the G-state (121.7 ppm) to the M-intermediate (126.8 ppm)

and the thermal decay process.

FIGURE 7. ^{13}C CP-MAS NMR signals of [20-^{13}C] retinal-*p*pR alone at -60 ºC under 4 kHz MAS. A. The difference spectra of the [20-^{13}C] retinal-*p*pR were obtained, (a) by subtracting the initial dark conditions (Dark1) from the green light illumination (520 nm) states (Green) (Green – Dark1), (b) by subtracting (Dark 1) from blue light (365 nm) illumination state (Blue) (Blue – Dark1) and (c) (Blue – Green). The difference spectrum shown in (a) indicates the transformation process from the G-state (13.6 ppm) to the M- (22.3 ppm), N'- (23.9 ppm) and O-intermediates (16.4 ppm) upon green light (520 nm) illumination. The difference spectra shown in (b) and (c) indicate that the O-intermediate (16.4 ppm) was trapped upon the subsequent blue light (365 nm) illumination. B. The difference spectra of [20-^{13}C] retinal-*p*pR obtained (d) (Blue – Dark1), (e) by subtracting the short dark conditions after turning off irradiation (Dark2) (Dark2 – Dark1) and (f) (Dark2 – Blue).

FIGURE 8. ^{13}C CP-MAS NMR signals of [14-^{13}C] retinal-*p*pR alone at -60 °C under 4 kHz MAS. A. The difference spectra of [14-^{13}C] retinal-*p*pR obtained (a) by subtracting the initial dark conditions (Dark1) from the green light (520 nm) illumination states (Green) (Green – Dark1), (b) by subtracting (Dark1) from the blue light (365 nm) illumination state (Blue) (Blue – Dark1) and (c) Blue – Green. The difference spectrum shown in (a) indicates the transformation process from the G-state (121.6 ppm) to the M-intermediates (127.1 ppm) upon green light (520 nm) illumination. The difference spectra shown in (b) and (c) indicate the transition process from the M-intermediates to the O-intermediate (115.4 ppm) upon subsequent blue light (365 nm) illumination. B. The difference spectra of [14-^{13}C] retinal-*p*pR obtained (d) by subtracting (Dark1) from (Blue) (Blue – Dark1), (e) by subtracting (Dark1) from the short dark conditions after turning off irradiation (Dark2) (Dark2 – Dark1) and (f) Dark2 – Blue. The difference spectra shown in (e) and (f) indicate that the remaining signal at 115.4 ppm belongs to the N'-intermediate.

FIGURE 9. The dependency of the chemical shift value of 20-^{13}C in retinal on the dihedral angles Φ and Ψ is shown in (A) and (B), respectively. In (A), only the dihedral angle Φ was rotated from the *trans* (-180º) to the *cis* (0º) configuration by setting Ψ and X at -175º and -66º, respectively (48). In (B), only the dihedral angle Ψ was rotated from the *anti* (-180º) to the *syn* (0º) configuration by fixing Φ and X to -177º and -66º, respectively (48). The calculated chemical shift values were converted

to ppm from TMS.

FIGURE 10. The chemical shift value of 14-^{13}C in retinal was calculated by changing the dihedral angle Ψ. The Φ angle was fixed at -150°, as estimated for the O-intermediate conformation discussed in Fig. 9. The X angle was set at the crystal conformation (48) of -66° in (▲), and the trans conformation (48) of -180° in (■).

FIGURE 11. The chemical shift value of 14-^{13}C in retinal was calculated by changing the dihedral angle Ψ and fixing Φ at -63°, as estimated for the N'-intermediate configuration discussed in Fig. 9. The X angle was set at the crystal configuration (48) of -66° in (▲) and the *trans* conformation (48) of -180° in (■).

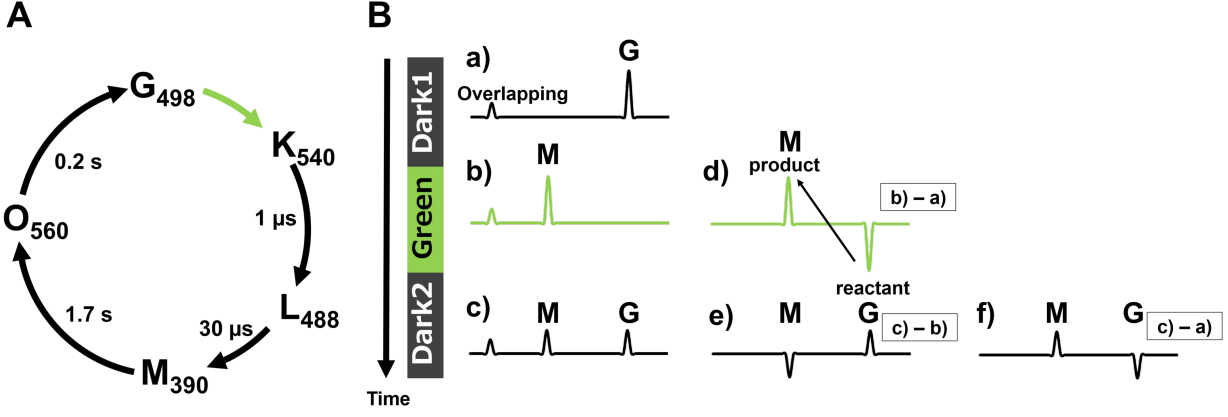
A
G498
K540
L488
M390
O560
0.2 s
1 µs
30 µs
1.7 s
B
Dark1
Green
Dark2
Time
a)
Overlapping
G
b)
M
c)
M
G
d)
M
product
b) – a)
reactant
e)
M
G
c) – b)
f)
M
G
c) – a)

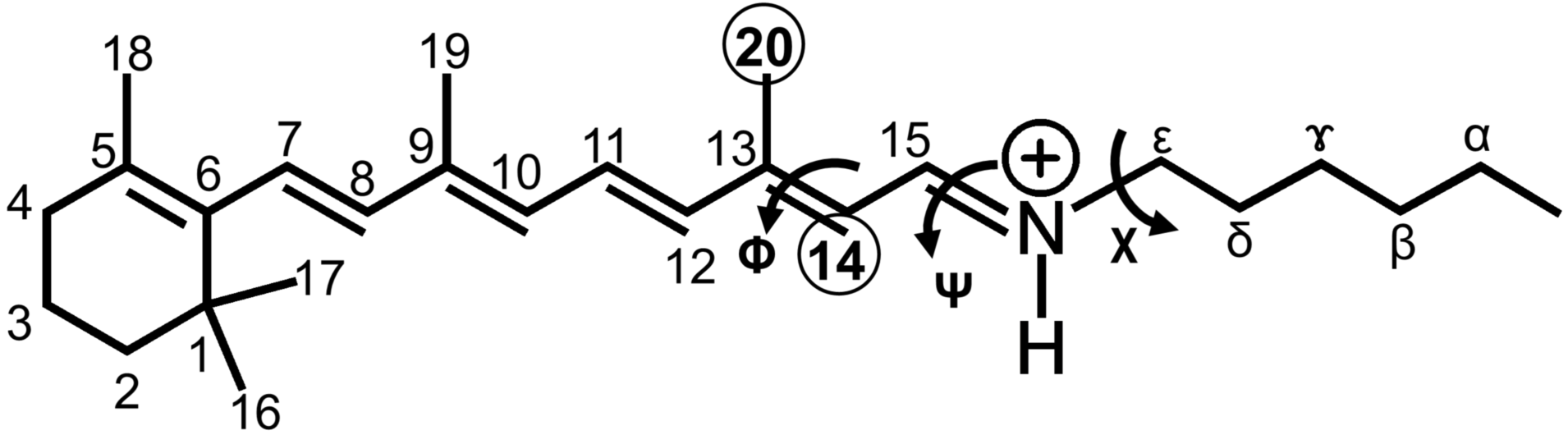
18
19
20
5
6
7
8
9
10
11
13
15
ε
γ
α
4
12
Φ
14
Ψ
N
χ
δ
β
17
3
1
H
2
16

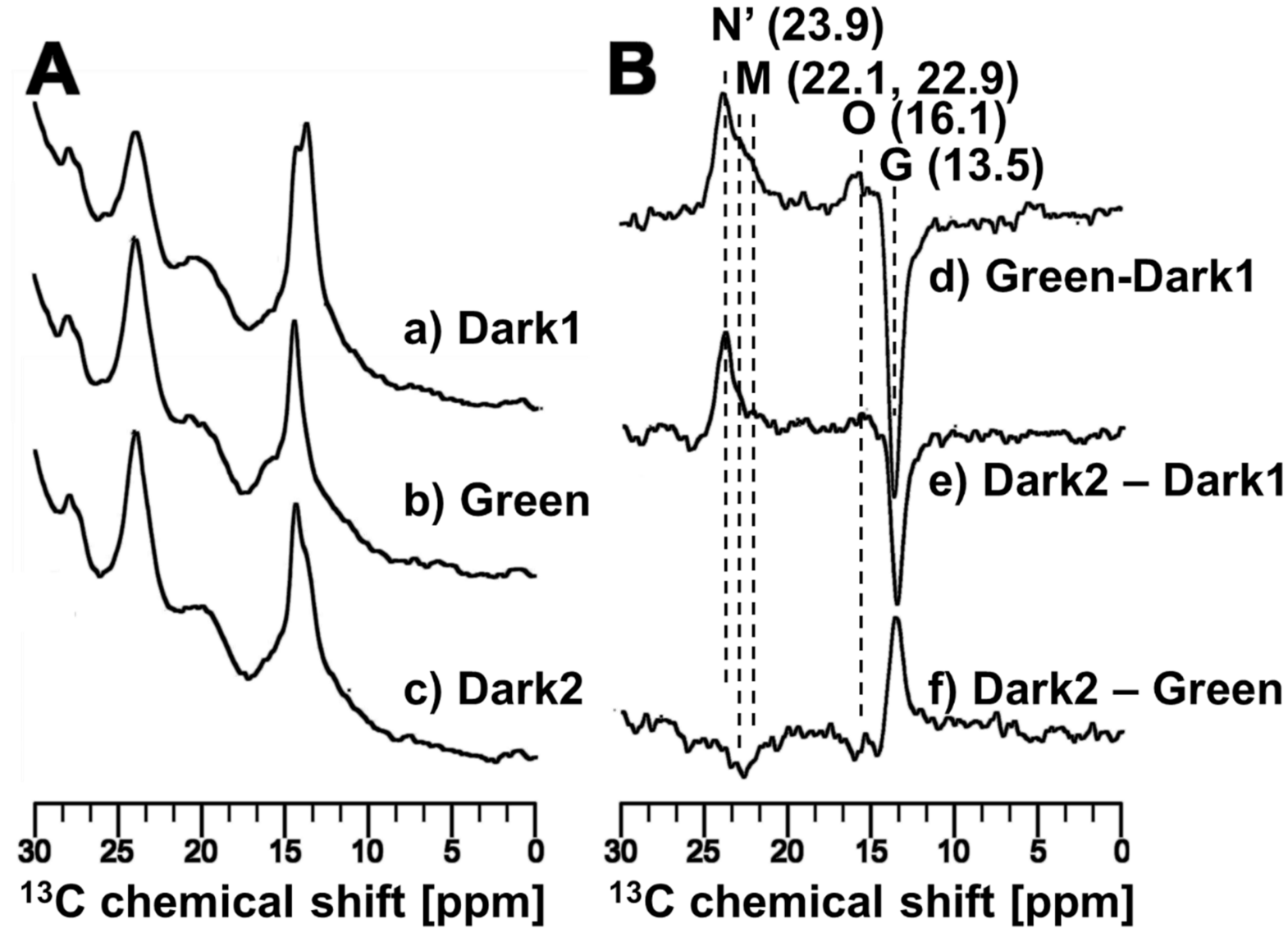
A
a) Dark1
b) Green
c) Dark2
30
25
20
15
10
5
0
13C chemical shift [ppm]
B
N' (23.9)
M (22.1, 22.9)
O (16.1)
G (13.5)
d) Green-Dark1
e) Dark2 – Dark1
f) Dark2 – Green
30
25
20
15
10
5
0
13C chemical shift [ppm]

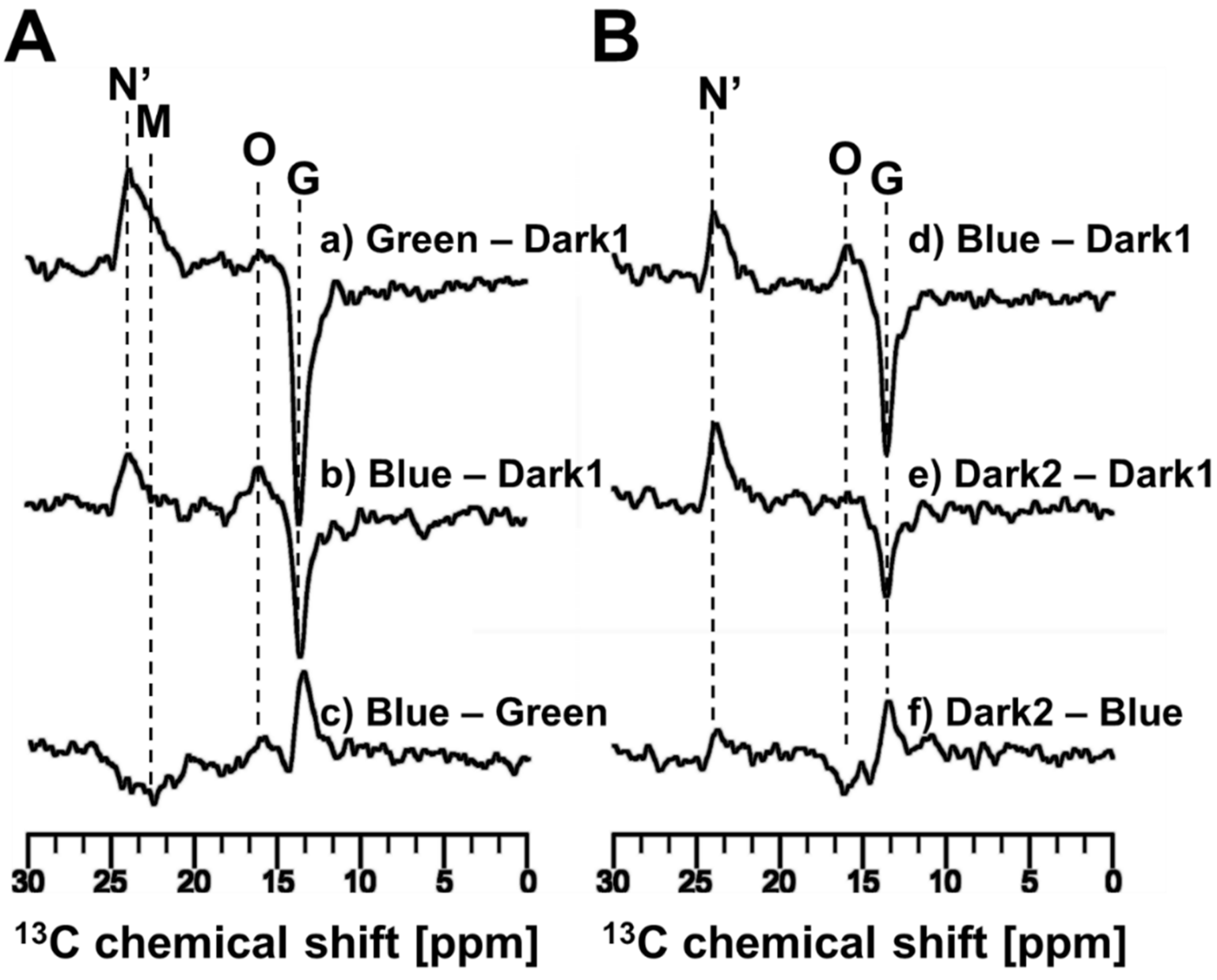
A
N'
M
O
G
a) Green – Dark1
b) Blue – Dark1
c) Blue – Green
30
25
20
15
10
5
0
13C chemical shift [ppm]
B
N'
O
G
d) Blue – Dark1
e) Dark2 – Dark1
f) Dark2 – Blue
30
25
20
15
10
5
0
13C chemical shift [ppm]

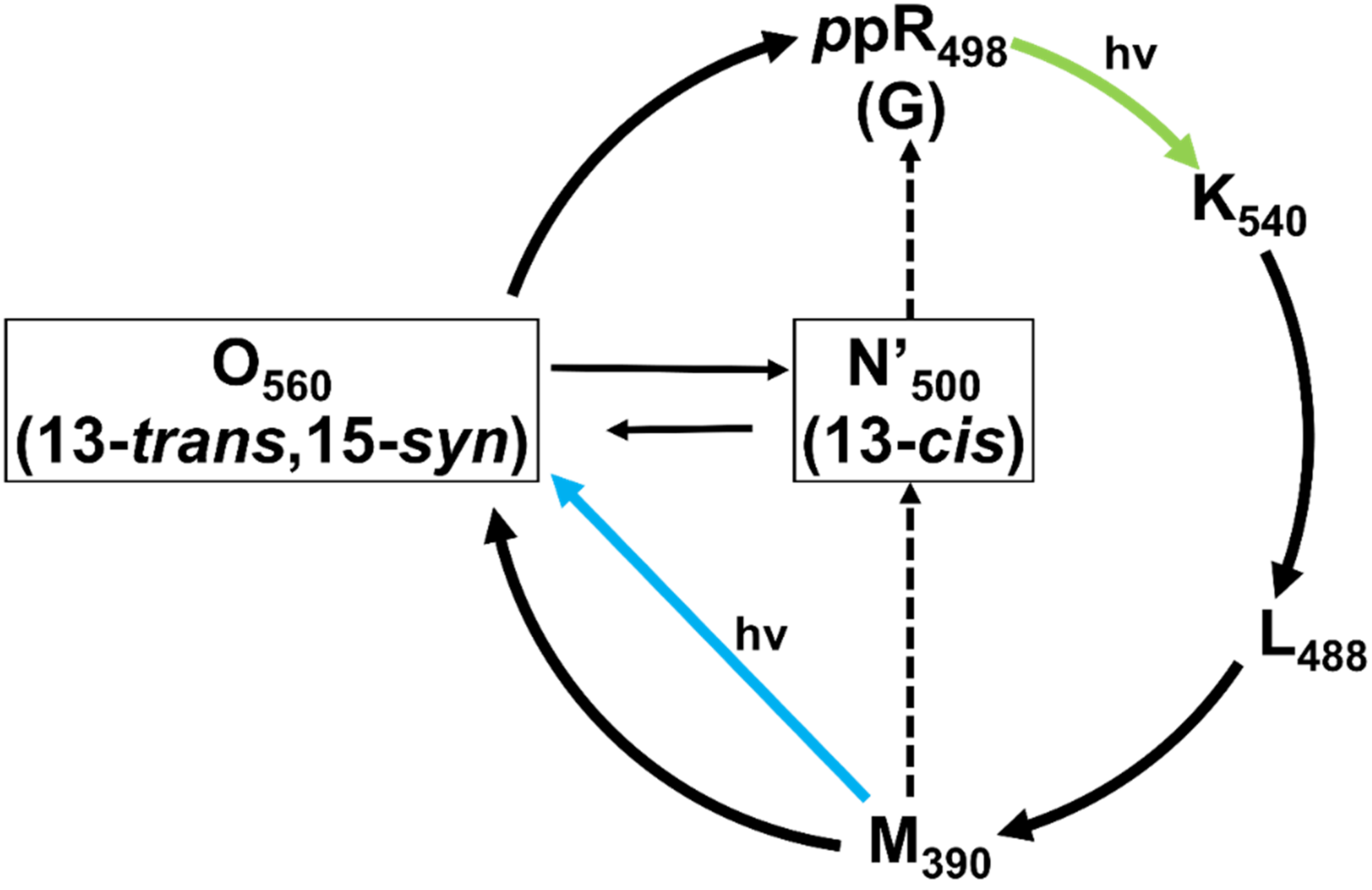
ppR498
(G)
hv
K540
O560
(13-trans,15-syn)
N'500
(13-cis)
L488
hv
M390

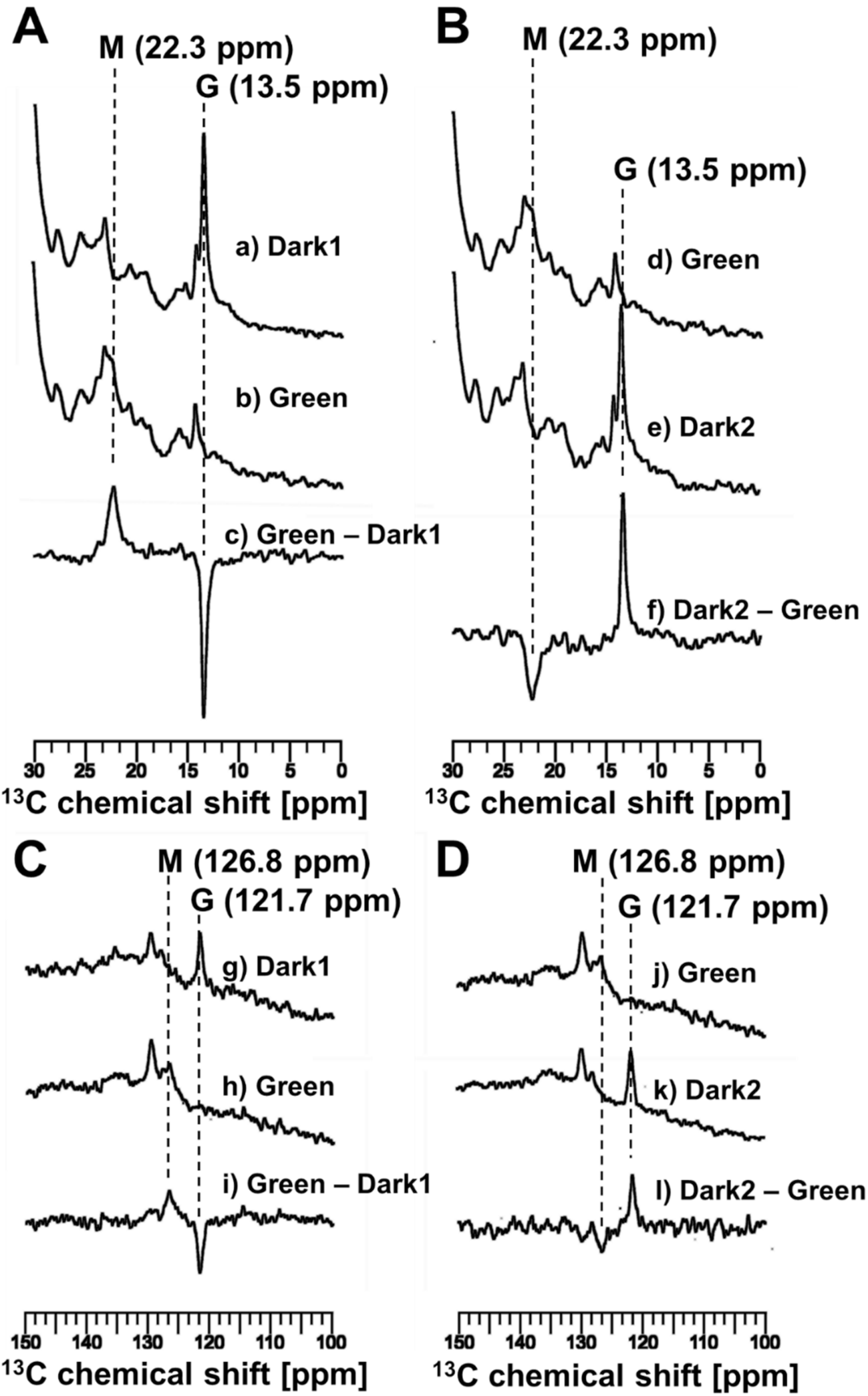
A
M (22.3 ppm)
G (13.5 ppm)
a) Dark1
b) Green
c) Green – Dark1
30 25 20 15 10 5 0
13C chemical shift [ppm]
B
M (22.3 ppm)
G (13.5 ppm)
d) Green
e) Dark2
f) Dark2 – Green
30 25 20 15 10 5 0
13C chemical shift [ppm]
C
M (126.8 ppm)
G (121.7 ppm)
g) Dark1
h) Green
i) Green – Dark1
150 140 130 120 110 100
13C chemical shift [ppm]
D
M (126.8 ppm)
G (121.7 ppm)
j) Green
k) Dark2
l) Dark2 – Green
150 140 130 120 110 100
13C chemical shift [ppm]

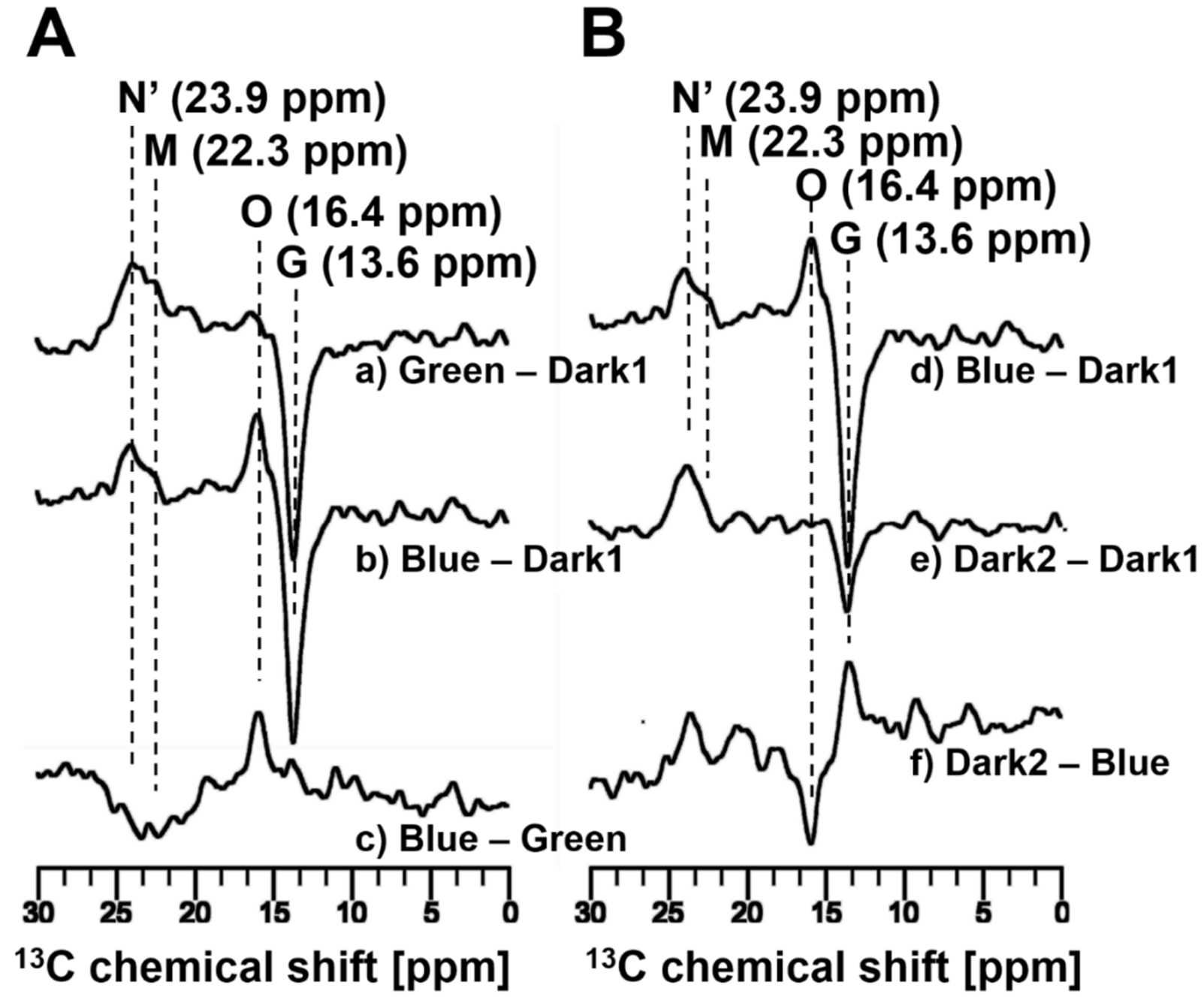
A
N' (23.9 ppm)
M (22.3 ppm)
O (16.4 ppm)
G (13.6 ppm)
a) Green – Dark1
b) Blue – Dark1
c) Blue – Green
30 25 20 15 10 5 0
13C chemical shift [ppm]
B
N' (23.9 ppm)
M (22.3 ppm)
O (16.4 ppm)
G (13.6 ppm)
d) Blue – Dark1
e) Dark2 – Dark1
f) Dark2 – Blue
30 25 20 15 10 5 0
13C chemical shift [ppm]

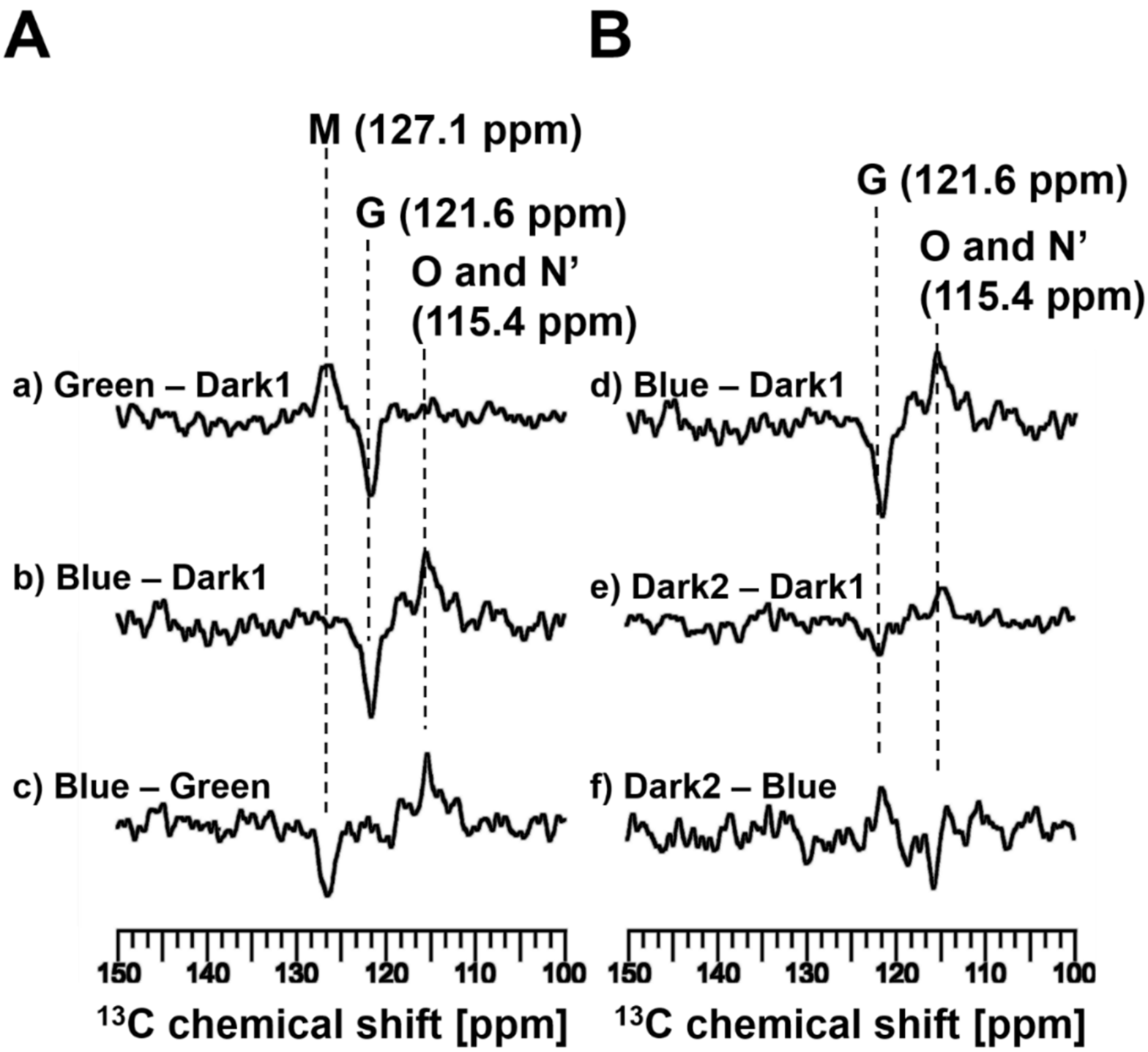
A
B
M (127.1 ppm)
G (121.6 ppm)
O and N'
(115.4 ppm)
a) Green – Dark1
b) Blue – Dark1
c) Blue – Green
G (121.6 ppm)
O and N'
(115.4 ppm)
d) Blue – Dark1
e) Dark2 – Dark1
f) Dark2 – Blue
150 140 130 120 110 100
^{13}C chemical shift [ppm]
150 140 130 120 110 100
^{13}C chemical shift [ppm]

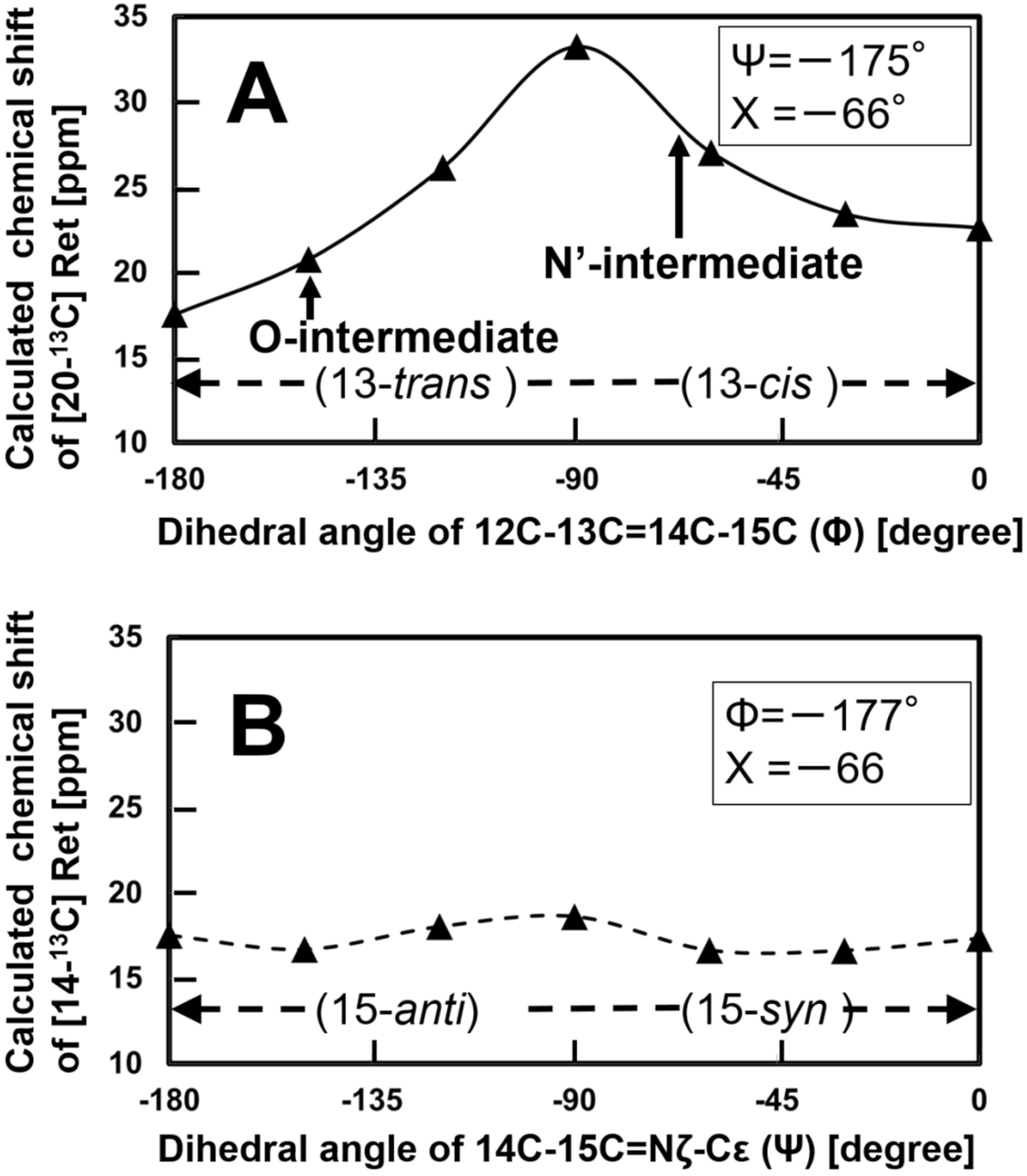
A
Ψ=−175°
X =−66°
N'-intermediate
O-intermediate
(13-trans)
(13-cis)
Calculated chemical shift of [20-13C] Ret [ppm]
35
30
25
20
15
10
-180
-135
-90
-45
0
Dihedral angle of 12C-13C=14C-15C (Φ) [degree]
B
Φ=−177°
X =−66
(15-anti)
(15-syn)
Calculated chemical shift of [14-13C] Ret [ppm]
35
30
25
20
15
10
-180
-135
-90
-45
0
Dihedral angle of 14C-15C=Nζ-Cε (Ψ) [degree]

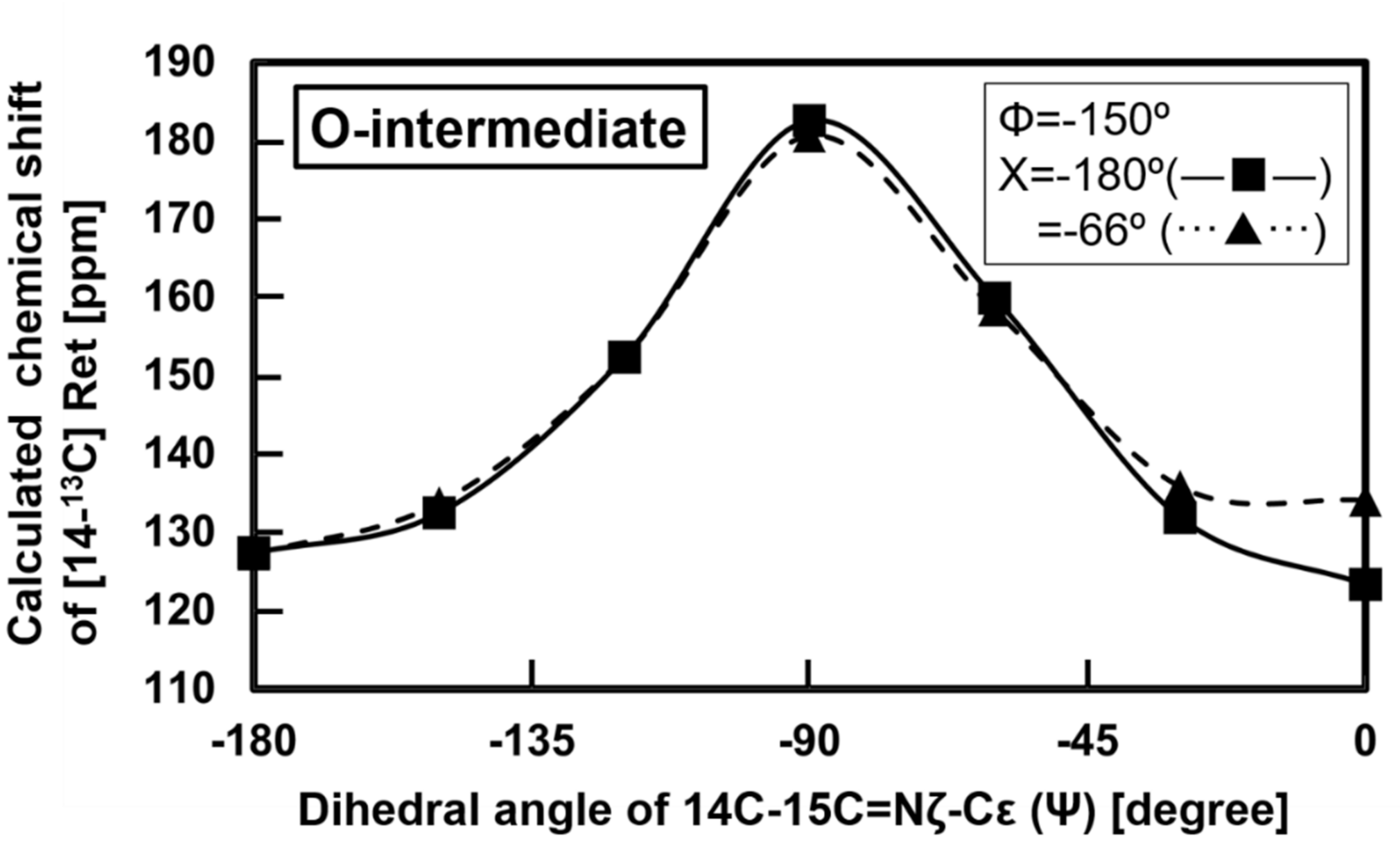
O-intermediate
Φ=-150º
X=-180º(—■—)
=-66º (···▲···)
Calculated chemical shift of [14-13C] Ret [ppm]
190
180
170
160
150
140
130
120
110
-180
-135
-90
-45
0
Dihedral angle of 14C-15C=Nζ-Cε (Ψ) [degree]

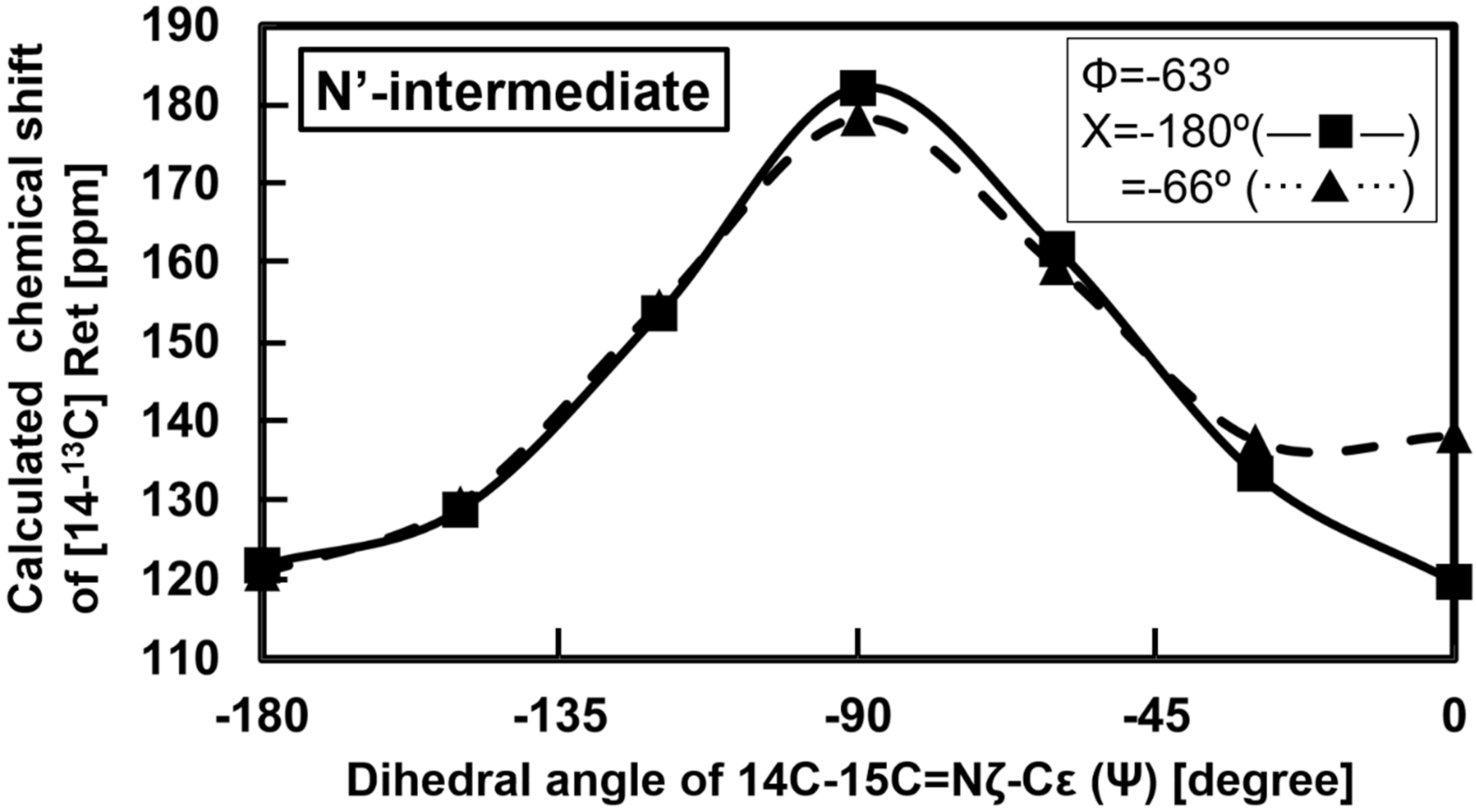
N'-intermediate
Φ=-63°
X=-180°(—■—)
=-66° (···▲···)
Calculated chemical shift of [14-13C] Ret [ppm]
190
180
170
160
150
140
130
120
110
-180
-135
-90
-45
0
Dihedral angle of 14C-15C=Nζ-Cε (Ψ) [degree]